Black Sea Journal of Engineering and Science
doi: 10.34248/bsengineering.1542181

Open Access Journal
e-ISSN: 2619 – 8991

Research Article
Volume 8 - Issue 1: xx-xx / January 2025

GENOTOXIC AND CYTOTOXIC EFFECTS OF NANOPARTICLE AND BULK FORMS OF MOLYBDENUM TRIOXIDE AND MOLYBDENUM DISULFIDE USED IN BIOIMAGING AND CANCER THERAPY

Nur KORKMAZ[1]*, Fatma ÜNAL[2], Ece AKBAŞ[2], Gökçe ÇALIŞ İSMETOĞLU[3], Deniz YÜZBAŞIOĞLU[2]

[1]*Gazi University, Graduate School of Natural and Applied Sciences, Teknikokullar, 06500, Ankara, Türkiye*
[2]*Gazi University, Faculty of Science, Department of Biology, Teknikokullar, 06500, Ankara, Türkiye*
[3]*Gazi University, Faculty of Science, Department of Chemistry, Teknikokullar, 06500, Ankara, Türkiye*

Abstract: Nanoparticles (NPs) and bulk forms of MoO_3 and MoS_2 (0.1, 1, 10, 100 µg/mL) used in cancer treatment and bioimaging were investigated by chromosome aberrations ('s' has been added), CBMN-Cyt and comet assay in human lymphocytes for the first time. This study compared both MoO_3 and MoS_2 and their NPs (two-dimensional (2D)) and bulk forms. Both NP and bulk forms of MoO_3 and MoS_2 did not cause an increase in the frequency of abnormal cell ('frequency' is moved to the left of 'abnormal cell') and CA/Cell compared to the control. While both NPs and bulk forms of MoS_2 significantly increased the micronucleus frequency, MoO_3 did not cause an increase. This increase was slightly higher in MoS_2 NPs than in their bulk form. According to our comet assay results, both NPs and bulk forms of the MoO_3 and MoS_2 significantly increased the DNA damage at all concentrations. Both MoO_3 and MoS_2 significantly decreased MI. Neither MoO_3 nor MoS_2 caused a significant variation in NDI, CBPI, % cytostasis, NPB, and NBUD frequency compared to the negative control. Both particles were also characterized physicochemically. Our results revealed that MoO_3 and MoS_2 may have weak genotoxic and cytotoxic effects. Therefore, the toxicity potential of these particles and their underlying mechanisms for safer usage need to be investigated in more detail by other *in vivo* ('in vivo' has been italicized) and *in vitro* genotoxicity and cytotoxicity tests.

Keywords: MoO_3, MoS_2, Genotoxicity, Cytotoxicity, Bioimaging, Cancer Therapy

***Corresponding author:** Gazi University, Graduate School of Natural and Applied Sciences, Teknikokullar, 06500, Ankara, Türkiye
E mail: nur.korkmaz1@gazi.edu.tr (N. KORKMAZ)

Nur KORKMAZ https://orcid.org/0000-0003-4969-2872
Fatma ÜNAL https://orcid.org/0000-0002-7468-6186
Ece AKBAŞ https://orcid.org/0000-0002-4978-3638
Gökçe ÇALIŞ İSMETOĞLU https://orcid.org/0000-0002-3369-6193
Deniz YÜZBAŞIOĞLU https://orcid.org/0000-0003-2756-7712

Received: September 03, 2024
Accepted: November 22, 2024
Published: January 15, 2025

Cite as: Korkmaz N, Ünal F, Akbaş E, Çalış İsmetoğlu G, Yüzbaşıoğlu D. 2025. Genotoxic and cytotoxic effects of nanoparticle and bulk forms of molybdenum trioxide and molybdenum disulfide used in bioimaging and cancer therapy. BSJ Eng Sci, 8(1): xxx-xxx.

1. Introduction

Cancer continues to be a significant cause of morbidity and mortality despite basic and clinical research and the testing of promising new treatments. Treatments such as chemotherapy, radiation therapy, immunotherapy, and targeted therapy used in cancer may induce oxidative stress through numerous free radicals that can attack cellular targets, leading to various side effects in biological systems. A lack of good selectivity, cytotoxicity, and multiple drug resistance also obstruct these therapies. Therefore, in recent years, non-traditional cancer treatments using nanotechnology and nanomedicine, a multidisciplinary field, have been applied for detection, diagnosis, and therapy (Indrakumar and Korrapati, 2020). Nanotechnology, thanks to its applications in diverse fields of medical science, has revolutionized the healthcare industry for bioimaging, diagnosis, and treatment of many fatal diseases, including cancer, by overcoming biological barriers in the body with nanosized drug carrier systems. One of the most promising candidates for developing more effective drugs is nanoparticles, the most effective strategies for early diagnosis and treatment of tumors and for controlling cancer development and progression (Verma et al., 2023). In particular, two-dimensional (2D) nanomaterials (NMs), including metal chalcogenides and oxides, have been increasingly used in sensors, catalysis, and biomedicine with their attractive physicochemical properties such as high surface-to-volume ratio and free surface energy levels (Li et al., 2021). Smaller than human cells, NPs are 1-100 nm in size, which allows them to enter live cells easily. Therefore, NPs can interact and/or rivalry with biological system cells and molecular components (Verma et al., 2023). Bulk forms (microparticles (MPs)) are substances between 1-1000 µm in properties compared to NPs. Both the designed NPs and MPs have many applications as next-generation biomedical agents in various biomedical fields such as

bioimaging, treatment of cancer and other diseases, biosensor, and drug and gene delivery. (Part of the sentence 'Both the cancer and other diseases, biosensor, and drug and gene delivery' has been deleted. This sentence has been added in full) (Kothaplamoottil Sivan et al., 2019; Indrakumar and Korrapati, 2020; Li et al., 2021; Wang et al., 2021; Sobańska et al., 2023). Molybdenum is one of the essential trace elements, similar to (Added space between 'similar' and 'to') boron, cobalt, copper, iron, and zinc, for humans', animals', and plants' lives. These elements are structural constituents (co-factors) of enzymes that carry out diverse functions such as regulating gene expression, antioxidant defense, and reproductive system, achieving immune functions, and preventing chronic diseases. Therefore, it is added to mineral supplements and fertilizers (Wang et al., 2021). In addition, the distinctive features of Mo-based nanomaterials, such as their relatively low toxicity, suitable catalytic activities (Kailasa et al., 2024), unique physicochemical properties, high surface-to-volume ratios, and their ability to serve as drugdelivery platforms for loading different types of chemotherapeutic drugs to achieve improved chemotherapy, made their use in various biomedical applications (Zhou et al., 2022). Semiconductor MoO_3 in the transition metal oxide group is one of the materials used in bioimaging and cancer treatment as a series of rising optothermal materials due to its ease of excretion, photoacoustic imaging capabilities, and surface plasmonicabsorption properties. The presence of inherent van der Waals voids in layered materials allows the easy incorporation of MoO_3 with varying guest species, presenting a strategy to optimize their physicochemical features and practice performance (Xing et al., 2020; Zhou et al., 2022). Considered all together, understanding the role of MoO_3 NPs in cancer and angiogenesis opens new avenues for nano-biological interference of selective cancer cell targeting with minimal damage to normal cells using natural trace elements being generally known to affect several metabolic enzymes (Indrakumar and Korrapati, 2020). It can efficiently kill cancer cells by generating reactive oxygen species (ROS) (Zhou et al., 2022). As a Mo-based compound, MoS_2 nanomaterials have recently attracted more attention in cancer diagnosis and treatment due to their unique physical and chemical properties. MoS_2 can adsorb various biomolecules and drug molecules through covalent or non-covalent interactions and is easy to be modified (Wang et al., 2021; Santos et al., 2023). MoS_2 NPs as a transition metal are preferred due to their large surface/volume ratio, distinct electronic characteristics, tunable band gap, high carrier mobility, friction, and catalytic and optical physio- chemical properties. MoS_2-nanocomposite can respond specifically to the tumor microenvironment, increasing drug accumulation at the tumor site, reducing side effects on non-cancerous tissues, and increasing the therapeutic effect. MoS_2 NPs are typically representative of 2D structures in the form of discs, plates, platelets, films, or sheets, similar to graphene, which is the most known 2D nanomaterial (Wang et al., 2021; Singh et al., 2024).

Since NPs and MPs are widely used in many areas, living beings are constantly exposed to these particles, and it is crucial to assess the toxicological effects of NPs and MPs comparatively to clarify the impact of different forms of the same material since the physicochemical and biological characteristics of NPs are different from those of the MPs, in general (Sobańska et al., 2023). For this reason, the genotoxic effects of NPs and MPs have been investigated with various *in vitro* and *in vivo* ('in vivo' has been italicized) test systems using different cell lines, primary cells, or (space added after the word 'organisms') organisms (Sobańska et al., 2023; Singh et al., 2024). The results of these studies revealed that while some particles have genotoxic potential, others do not. In the case of NPs and MPs of molybdenum trioxide and molybdenum disulfide, both positive and negative genotoxic results have been reported following both *in vitro* and in vivo studies (Asadi et al., 2019; Sobańska et al., 2020a; Kumari and Mangala, 2022; García-Carpintero et al., 2023; Santos et al., 2023). Due to insufficient and contradictory data in the literature, the toxic, especially genotoxic, effects of NPs and MPs of molybdenum trioxide and molybdenum disulfide need more detailed investigation with numerous test systems using various cell types. Chromosome aberrations (CAs), cytokinesis-block micronucleus cytome (CBMN-Cyt), and comet (single-cell gel electrophoresis-SCGE) assays are valuable biomarkers in determining the genotoxicity/cytotoxicity potential of various agents (Bakhoum and Cantley, 2018; Fenech et al., 2020; Mamur et al., 2022; Collins et al., 2023). Therefore, we aimed to investigate, for the first time, the genotoxic and cytotoxic potential of NPs and MPs of molybdenum trioxide and molybdenum disulfide on human lymphocytes *in vitro* using CAs, CBMN-Cyt, and comet assays. To our knowledge, no data have yet been published on these two NPs and MPs by assays as mentioned earlier in human lymphocytes as genotoxicity and cytotoxicity biomarkers.

2. Materials and Methods

2.1. Materials

In this research, the peripheral blood was obtained from three healthy volunteers, two women and one man (<30 years old), who had no health problems, did not smoke, did not consume alcohol, and had not taken any medication in the last three months.

2.1.1. Test materials

All NPs and MPs were obtained from Nanografi (Türkiye). The information given by the company is as follows: the size of MoO_3 NPs is 10-80 nanometers (99% purity) (Cas No: 1313-27-5), the particle size of MoO_3 MPs is 325 mesh (Cas No: 1313-27-5) and their shapes are nearly spherical. The mean size of MoS_2 NPs is 100 nanometers, its shape is spherical, and its purity is

99.95% (Cas No: 1313-33-5); the particle size of MoS_2 MPs is 325 mesh. Its shape is flaky and 99.9% pure (Cas No: 1313-33-5).

2.1.2. Chemicals

Methyl alcohol (CAS No: 67-56-1), glacial acetic acid (CAS No: 64-19-7), Giemsa (CAS No: HX947066), NaOH (Catalog No: 1310-73-2), Buffer tablets pH 6.8 (CAS No: 111374) and Entellan (CAS No: 1079610500) were obtained from Merck. Mitomycin-C (CAS No: 200-008-6), colchicine (CAS No: 64-86-8), and cytochalasin-B (CAS No: 14930-96-2) were obtained from Sigma. DMSO (CAS. No: 67-68-5), EDTA (CAS. No: 6381-92-6), triton X-100 (CAS. No: 9002-93-1), low melting agarose (CAS. No: 9012-36-6), tris (CAS. No: 77-86-1), agarose low EEO (CAS. No: 9012-36-6), H_2O_2 (CAS. No: 7722-84-1), ethidium bromide (CAS No: 1239-48-8), Tris (CAS No: 77-86-1), Triton X-100 (CAS No: 9002-93-1) and formaldehyde (CAS No: 50-00-0) were supplied from Applichem. LymphoPlus (Catalog No:CY100-100), Dulbecco's PBS (Catalog No: PBSH0500-540), and Lymphocyte separation medium (Catalog No: J0100-840) were obtained from Cegrogen Biotech. Trypan Blue (CAT No: L 6323) was supplied from Biochrom.

2.2. Characterization of NPs and MPs of MoO_3 and MoS_2

The shape and particle size of both NPs and MPs of MoO_3 and MoS_2 were examined by transmission electron microscopy (TEM) (JEOL JEM-2100PLUS) at 200 kV and scanning electron microscopy (SEM) (ZEISS EVO40) at 5.00-10.00 kV at Yeditepe University SEM/TEM Imaging Laboratory. All particles were suspended in double distilled water (DDW), homogenized in an ultrasonic bath (100 W, 50-60 kHz, J.P. Selecta) for 10 minutes, and transferred to a carbon-coated copper grid with a pipette for TEM. For SEM, particles were coated with gold after transfer to double-sided tape on the stubs. The particles were photographed, and 50 were randomly measured with the Image J program to determine the average diameter. The zeta potential (mV) (as a measure of surface charge) was determined by dynamic light scattering (DLS). Hydrodynamic diameter (HD) and polydispersity index (PDI) of MoO_3 NPs and MoS_2 NPs were obtained using a Zeta-sizer Nano-ZS instrument (Malvern, Worcestershire, UK) equipped with a 4-mW He-Ne laser operating at λ=633 nm and a noninvasive backscatter system (NIBSTM) which measures the light scattered at a backscatter angle of 173°. Before measurement, all samples were suspended in DDW (HD-0.5 g/L, ζ-potential-0.1 g/L) and homogenized in an ultrasonic bath at 10 min. All analyses were measured using the Malvern Zeta-sizer Nano-ZS (Worcestershire, UK) by photon correlation spectroscopy for HD (10^{-3} M ('-3' has been superscripted) NaCl (aq) (0.1 g/L) at 25°C) and by laser Doppler electrophoresis technique for zeta potential. All samples were transferred to zeta cells and placed in the chamber at about 1 mL for measurement (Kizilkaya et al., 2023).

2.3. Preparation of Test Suspensions

Application concentrations (0.1, 1, 10, and 100 µg/mL) of NPs and MPs of molybdenum trioxide and molybdenum disulfide were diluted in DDW from their stock suspensions that were sonicated for 30 minutes. Following serial dilutions, all suspensions were sonicated for another 10 minutes. Before addition to the cell culture medium, all concentrations of NPs and MPs were homogenized using a vortex for 1 minute.

2.4. Selection of Test Concentrations

Literature searches were carried out and considered as the first reference to determine the concentrations to be used in this study. LD_{50} of MoO_3 was 1831.25 ppm in the HepG2 cell line, 193.91 ppm in the HEK 293 cell line (Kothaplamoottil Sivan et al., 2019), 2.689 mg/kg in rat oral intake, 106±73.79 mg/kg in the rat heart, 136±99.42 mg/kg in rat liver, 143±44 mg/kg in rat kidney and 107±595 mg/kg in rat stomach (Akhondipour et al., 2018). Additionally, the LD50 dose was reported as 242 mg/kg in the rat oral toxicity data program PROTOX (Sharma et al., 2020). It has been observed that toxicity studies in the literature range between 0.25 and 5000 µg/mL (Kothaplamoottil Sivan et al., 2019; Sharma et al., 2020). Toxicity values determined for MoS_2 in the literature were between 0.1 and 1000 µg/mL (Appel et al., 2016; Desai et al., 2020). MoS_2 caused toxic effects in 10 and 100 µg/mL in *Eisenia fetida* (Sun et al., 2023), 5-20 µg/mL on human lung epithelial cells (Sahoo et al., 2022), 0-100 µg/mL in Kupffer cells (Li et al., 2021). In another study, the LD_{50} value was reported as 1 mg/kg (intraperitoneal) in Swiss albino rats (Yadav et al., 2021). Depending on these data, a preliminary dose range finder test was carried out with the concentrations of 0.1, 1, 5, 10, 20, 25, 50, 75, 100, 150, 200, 250, 300, 350, 400, 450 and 500 µg/mL in human lymphocytes using mitotic inhibition test (EC_{50}). In the preliminary trial, toxic effects were observed at concentrations above 300 µg/mL, which differed from some of the data in the literature. The cytotoxic effects of concentrations between 100 and 300 µg/mL were not significantly different. Therefore, we decided to apply 0.1, 1, 10, and 100 µg/mL for both MoO_3 and MoS_2.

2.5. Chromosome Aberration Test

The chromosome aberration assay was applied using Evans's method (1984) with some modifications (Yüzbaşioğlu et al., 2006). In this assay, 200 µL of 1/10 heparinized peripheral blood was added to a 2.5 mL chromosome medium. The incubation was carried out at 37ºC for 72 h. The cells were treated with four concentrations (0.1, 1, 10, and 100 µg/mL) of either NPs or MPs of molybdenum trioxide and molybdenum disulfide for 24 and 48 hours. A negative (distilled water) and a positive control (Mitomycin-C, MMC, 0.20 µg/mL) were also included. 0.06 µg/mL colchicine was added into each culture 2 hours before cell harvesting. The cell suspension was centrifuged for 10 min, treated with hypotonic solution (KCl, 0.075M) for 20 min at 37°C, and then fixed in cold and fresh fixative (methanol: glacial acetic acid, 3:1, v/v). Finally, metaphase spreads were prepared by dropping the cell suspension onto slides.

Slides prepared for CAs were stained with 5% Giemsa (pH 6.8) for 20-25 min, dried at room temperature, and mounted with entellan.

2.6. Cytokinesis-Block Micronucleus Cytome Test (added capitalization of the letter 'b')

The cytokinesis-block micronucleus cytome (CBMN-Cyt) test was applied with some modifications in the method of Fenech (2000; 2007) (Kirsch-Volders et al., 2011). 200 µL of 1/10 heparinized peripheral blood samples were added into a 2.5 mL chromosome medium and incubated for 72 h at 37°C. The cells were treated with four concentrations (0.1, 1, 10, and 100 µg/mL) of NPs and MPs of molybdenum trioxide and molybdenum disulfide for 48 hours. Cytochalasin-B (5.2 µg/mL) was added to arrest the cytokinesis at the 44th hour of incubation (Fenech, 2007). A negative (distilled water) and a positive control (Mitomycin-C, MMC, 0.20 µg/mL) were also maintained. Following incubation, the cultures were treated with hypotonic solution (0.075M KCl for 5 min at +4 °C) and then fixed in cold and fresh fixative (methanol: glacial acetic acid, 3:1, v/v) supplemented with formaldehyde according to the method of Palus et al. (2003). The slides were then stained with 5% Giemsa at room temperature.

2.7. Comet Assay

To determine the DNA-damaging effect of NPs and MPs of MoO_3 and MoS_2 on human lymphocytes, the comet assay was applied using Singh et al.'s (1988) protocol with some modifications (Akbas et al., 2022). Isolated lymphocytes by suspending blood specimens in PBS were then treated with four different concentrations (0.1, 1, 10, and 100 µg/mL) of the NPs and MPs of MoO_3 and MoS_2 for 1 and 3 hours at 37°C. A negative (sterile distilled water) and a positive (100 µM H_2O_2) controls were also maintained. A trypan blue test was conducted for cell viability, which was >75% for all treatment groups. Lymphocytes in suspension were centrifuged and then resuspended in PBS. The mixture of cell and low melting point agarose (1:1) was gently layered onto the slides precoated with normal melting agarose (%1). Slides were covered with a cover slip and kept in a cold lysing solution (2.5M NaCl, 100 mM EDTA, 10 mM Tris pH=10, comprising %10 DMSO and %1 Triton X-100) for at least 1 h. Slides were electrophoresed for DNA unwinding at 25V, 300 mA for 20 min in electrophoresis buffer (10M NaOH+ 0.2M EDTA+ distilled water). At the end, slides were neutralized in 0.4 M Tris (pH 7.5) for 15 mins and then stained with ethidium bromide (20 µg/mL). this part will be deleted

2.8. Cell Scoring

In the CAs test, 100 well-spread metaphases from each donor (a total of 300 metaphases) were analyzed to determine the frequency of CAs and CAs/cell for each treatment. To determine the mitotic index (MI=the frequency of cells undergoing mitosis among the total number of cells examined), 1000 cells from each donor (total 3000 cells) were evaluated. In the CBMN-Cyt assay, a total of 3000 binucleated cells (1000 cells per donor) were analyzed for each treatment to determine the frequency of micronucleus, nucleoplasmic bridge (NPB), and nuclear bud (NBUD). To evaluate the nuclear division index (NDI), a total of 1500 cells (500 cells per donor) were scored, and the following formula was used: NDI=[1xM1+2xM2+3xM3+4xM4]/N, where M1-M4 represent the number of cells with 1-4 nuclei, respectively, and N is the total number of cells examined (Michalová et al., 2020). Cytokinesis block proliferation index (CBPI) was evaluated from a total of 1500 cells (500 cells for each donor) by the following formula: [(1xnumber of mononuclear cells) + (2x number of binuclear cells) + (3x number of multinuclear (3 and more) cells)/ n(total number of cells) (Lorge et al., 2008). The percentage of cytostasis was also determined using the following formula: % cytostasis: 100-100 [(CBPIT-1): (Added space between C and parenthesis) (CBPIC-1)]; where T stands for test substance, and C stands for control (Lorge et al., 2008). In comet assay, a total of 300 cells (50 cells x² slides)/donor were analyzed for each treatment and control group under a fluorescence microscope (Olympus BX51, Japan) equipped with an excitation filter (546 nm) and a barrier filter (590 nm) using a specialized image analysis system (Comet Assay IV, Perceptive Instruments Ltd., Haverhill, UK).

2.9. Statistical Analyses

To determine the statistical difference between treated and untreated cells, the z-test was used for the frequency of abnormal cells, CAs/Cell, MI, frequency of MN, NPB, NBUD, NDI, CBPI, and % cytostasis. T-test was applied for comet scores. The regression analysis was performed to determine concentration-response relationships by using the SPSS 22.0 program.

3. Results

3.1. Characterization of NPs and MPs of MoO_3 and MoS_2

The results of electron microscopy and DLS measurements (HD, PDI and zeta potential) were given in Table 1. TEM/SEM images of the particles supplied by the company revealed that while the shape of the MoO_3 NPs is formed from a mixture of spherical and ellipsoid, MoO_3 MPs are lamellar in structure, (Cas No: 1313-27-5). The shape of the MoS_2 NPs is mainly lamellar in structure, and MoS_2 MPs are mainly formed from lamellar structure, but some particles are also present and distributed homogeneously (Cas No: 1313-33-5). In this research we also determined the shape of these NPs (2D) and MPs. SEM and TEM images in Figure 1 revealed that the(shape of the MoO_3 NPs is formed from a mixture of spherical, ellipsoid, and rod-like particles, while MoO_3 MPs are formed from a mixture of lamellar, ellipsoid, and rod-like particles. On the other hand, the shape of MoS_2 NPs consists of a mixture of lamellar, ellipsoidal, and spherical particles. MoS_2 MPs consist of rod, lamellar, and ellipsoidal structures.

3.2. Cytotoxicity

The present study showed that MoO_3 NPs significantly and

dose-dependently decreased the mitotic index in all concentrations (except 1 µg/mL) at 24-h treatment (r= -0.87) (Figure 3). At 48-h treatment, these NPs also significantly decreased the mitotic index at all concentrations (except 100 µg/mL) (r=-0.15) (Figure 4).

Table 1. Electron microscopy and DLS characterization of test chemicals

	Average length (nm)	Average diameter (nm)	The smallest size (nm)	The largest size (nm)	Zeta potential (mV)	Hydrodynamic diameter (HD) (nm)	HD Intensity (%)	Polydispersity index
MoO_3 NPs	697.46	631.64	40	2486	-34.5±9.91	423.2±75.54	100.0	0.704
MoO_3 MPs	32030	24745.52	3162	70228	-16.1±4.32	-	-	-
MoS_2 NPs	928	644.12	74	6036	-27.9±7.18	484.9±39.33	100.0	0.958
MoS_2 MPs	14858.98	10086.10	1967	46920	-14.2±5.94	-	-	-

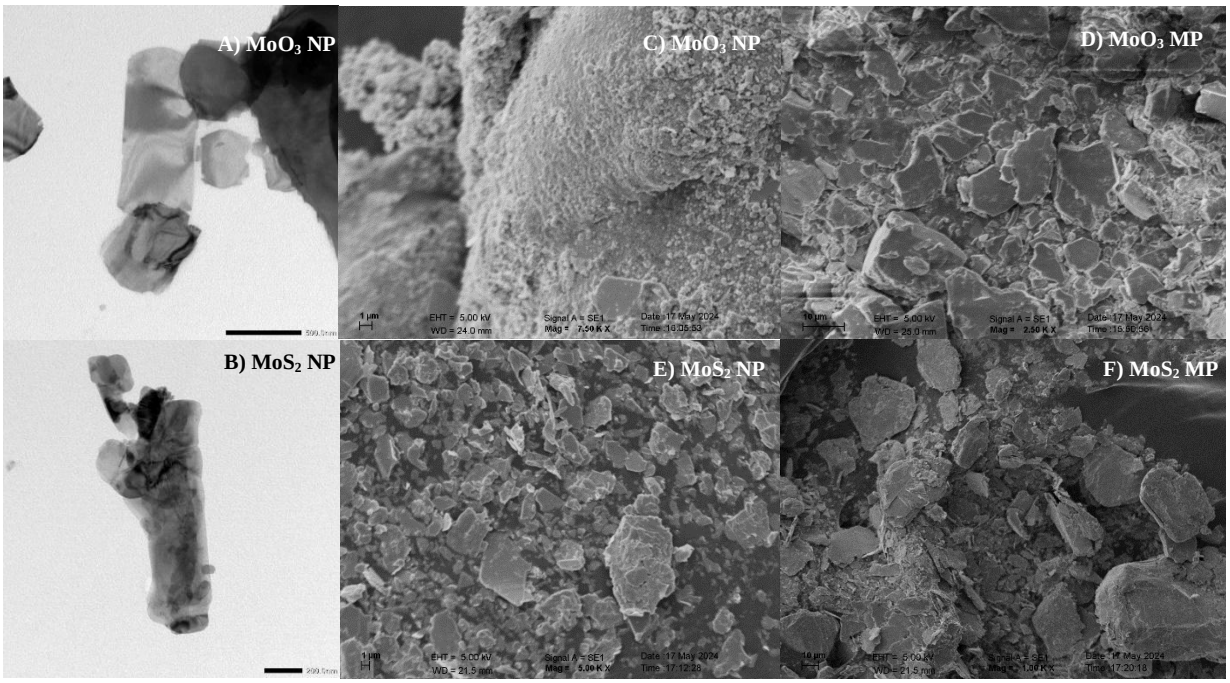

Figure 1. TEM images of MoO_3 and MoS_2 NPs (A and B) and SEM images of MoO_3 and MoS_2 MPs (C, D, E and F).

MoO_3 MPs also reduced the mitotic index significantly and dose-dependently at all concentrations at both 24 h (r=-0.78) and 48 h (r=-0.88) treatments (Figure 3 and Figure 4). Similarly, MoS_2 NPs declined the mitotic index at all concentrations at both 24- (except 1 µg/mL) (r= -0.70) and 48-h (r=-0.47) treatments with high and low concentration-dependently, respectively (red place will be deleted) . MoS_2 MPs reduced the mitotic index in a slightly dose-dependent manner at 1 and 100 µg/mL concentrations at both 24- (r=-0.49) and 48-h (r=-0.75) treatments (Figure 5 and Figure 6). In the present study, none of the test materials significantly altered NDI, CBPI, and % cytostasis and did not affect cell proliferation.

3.3. Chromosome Aberration Test Results of NPs and MPs of MoO_3 and MoS_2

In this study, the genotoxic effect of MoO_3 and MoS_2 NPs and MPs were evaluated using the CA test in human lymphocytes *in vitro*, and the results were given in Tables 2 and 3. While a few concentrations of both NPs and MPs slightly increased the frequency of abnormal cells and CAs/Cell in human lymphocytes at both 24 h and 48 h treatments, none was significant compared to the negative control. A few concentrations revealed the same frequency as the respective negative control. While 10 µg/mL concentration of MoO_3 NPs at 48 h application did not induce any structural aberration, other concentrations induced only one, two, or scarcely three structural aberrations in lymphocytes. Interestingly, all the concentrations of both MoO_3 NPs and MPs at 24 h treatment and MoS_2 NPs at 48 h treatment generated polyploidy.

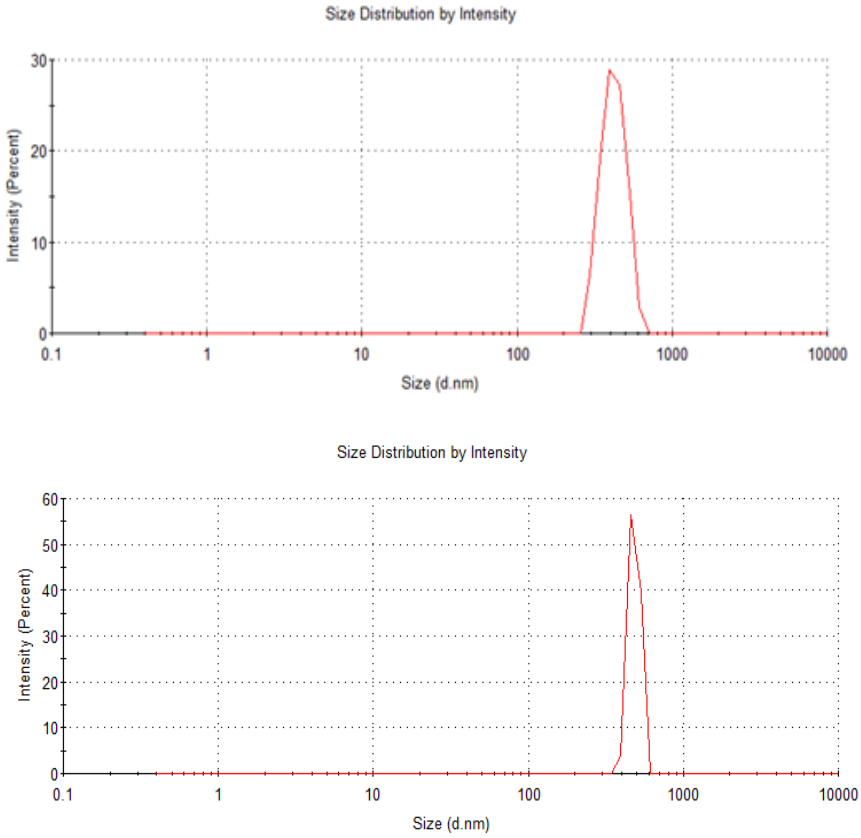

Figure 2. Frequency curve of (a) hydrodynamic diameter of MoO_3 NPs and (b) hydrodynamic diameter of MoS_2 NPs.

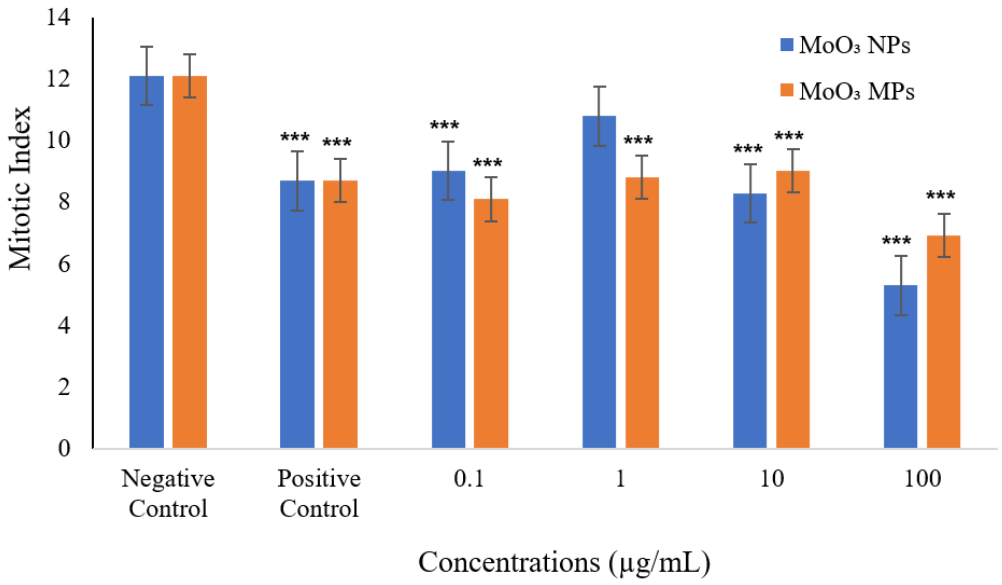

Figure 3. The frequency of MI in human lymphocytes exposed to MoO_3 NPs and MPs for 24 h. ***Significantly different from the control P<0.001(z test).

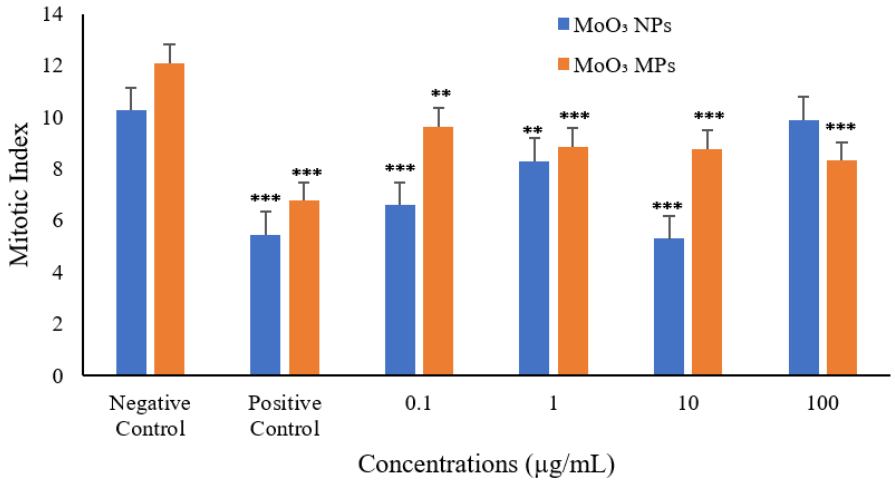

Figure 4. The frequency of MI in human lymphocytes exposed to MoO_3 ('3' was made a subscript)NPs and MPs for 48 h.** (**' was made a subscript) Significantly different from the control P<0.01 (z test). ***Significantly (**' was made a subscript) different from the control P<0.001(z test).

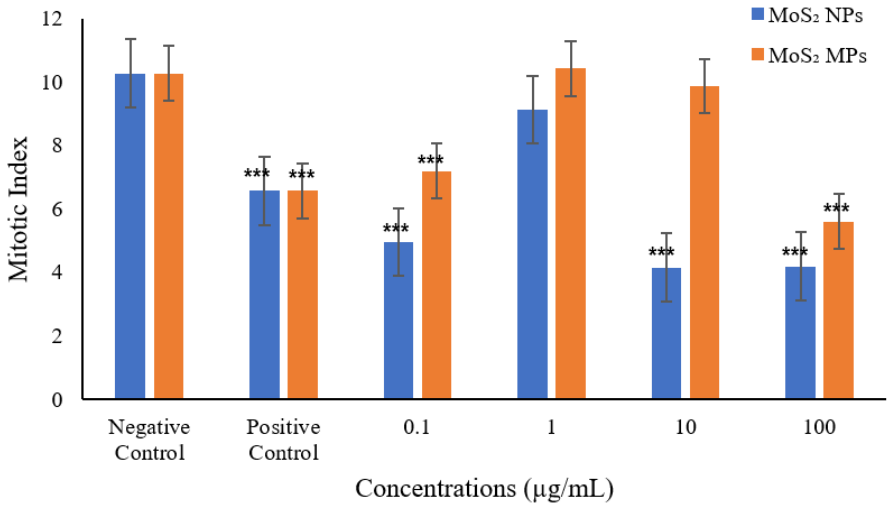

Figure 5. The frequency of MI in human lymphocytes exposed to MoS_2 NPs and MPs for 24 h. ***Significantly (**' was made a subscript) different from the control P<0.001(z test).

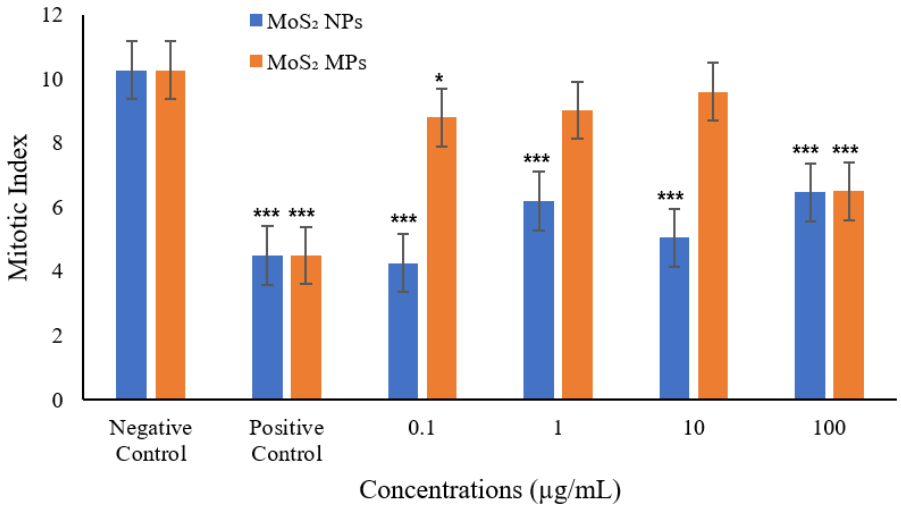

Figure 6. The frequency of MI in human lymphocytes exposed to MoS_2 ('2' was made a subscript)NPs and MPs for 48-h. *Significantly different from the control P<0.05 (z test). ***Significantly different from the control P<0.001(z test).

Table 2. Effects of NP_S and MPs of MoO_3 on CAs frequency in cultured human lymphocytes

Test substance	Treatment		Aberrations								Abnormal cell ± SE (%)	CAs/Cell ± SE
	Time (h)	Concentration (µg/mL)	ctb	csb	f	dic	scu	ex	p	en		
NC	24	0.00	1	-	-	-	-	-	-	-	0.33±0.11	0.003±0.003
PC (MMC)	24	0.20	11	1	-	-	4	1	8	-	8.33±1.60***	0.080±0.016***
MoO_3 NP_S	24	0.1	2	-	-	-	-	-	1	-	1.00±0.57	0.010±0.005
		1	-	-	-	-	-	-	1	-	0.33±0.33	0.003±0.010
		10	-	-	-	-	-	-	2	-	0.67±0.47	0.007±0.004
		100	-	-	-	-	-	-	2	-	0.67±0.47	0.007±0.004
MoO_3 MP_S	24	0.1	-	-	-	-	-	-	3	-	1.00±0.57	0.010±0.005
		1	-	-	-	-	-	-	2	-	0.67±0.47	0.007±0.004
		10	-	-	-	-	-	-	1	-	0.33±0.33	0.003±0.010
		100	2	-	-	-	-	-	1	-	1.00±0.57	0.010±0.005
NC	48	0.00	1	-	-	-	-	-	-	-	0.33±0.11	0.003±0.003
PC (MMC)	48	0.20	12	3	1	-	1	4	9	3	11,00±1,81***	0.110±0.017***
MoO_3 NP_S	48	0.1	1	-	1	-	-	-	1	-	1.00±0.57	0.010±0.005
		1	-	-	1	-	-	-	-	-	0.33±0.33	0.003±0.010
		10	-	-	-	-	-	-	-	-	0.00±0.00	0.000±0.000
		100	1	-	1	-	-	-	-	-	0.67±0.47	0.007±0.004
NC	48	0.00	1	-	-	-	-	-	-	-	0.33±0.11	0.003±0.003
PC (MMC)	48	0.20	11	5	-	1	3	1	7	-	9,33±0,55***	0,090±0,020***
MoO_3 MP_S	48	0.1	-	-	-	-	-	-	1	-	0.33±0.33	0.003±0.010
		1	2	-	-	-	-	-	-	-	0.67±0.47	0.007±0.004
		10	-	-	-	-	-	-	-	1	0.33±0.33	0.003±0.010
		100	-	-	-	-	-	-	-	1	0.33±0.33	0.003±0.010

ctb= chromatid break, csb= chromosome break, f= fragment, dic= dicentric chromosome, scu= sister chromatid union, ex= chromatid exchange, p= polyploidy, en= endoreduplication, SE= standard error, PC (MMC)= positive control- mitomycin C, NC= Negative control, ***Significantly different from the negative control P<0.001 (z test)

Table 3. Effects of NP_S and MPs of MoS_2 on CAs frequency in cultured human lymphocytes

Test substance	Treatment		Aberrations								Abnormal cell ± SE (%)	CAs/Cell ± SE
	Time (h)	Concentration (µg/mL)	ctb	csb	f	dic	scu	ex	p	en		
NC	24	0.00	-	-	-	-	-	-	-	-	0.00±0.00	0.000±0.000
PC (MMC)	24	0.20	10	7	3	-	2	5	3	-	10.00±1.73***	0.100±0.017***
MoS_2 NP_S	24	0.1	1	-	-	-	-	-	1	1	1.00±0.57	0.010±0.005
		1	2	-	-	-	-	-	1	-	1.00±0.57	0.010±0.005
		10	1	-	-	-	-	-	-	-	0.33±0.33	0.003±0.010
		100	-	-	-	-	-	-	-	-	0.00±0.00	0.000±0.000
MoS_2 MP_S	24	0.1	2	-	-	-	-	1	2	-	1.67±0.73	0.020±0.008
		1	-	-	-	-	-	-	-	-	0.00±0.00	0.000±0.000
		10	-	-	-	-	-	-	1	-	0.33±0.33	0.003±0.003
		100	1	-	-	-	-	-	-	-	0.33±0.33	0.003±0.003
NC	48	0.00	2	-	-	-	-	-	-	-	0.67±0.47	0.006±0.004
PC (MMC)	48	0.20	12	10	1	3	4	2	2	-	11.33±1.83***	0.120±0.019***
MoS_2 NP_S	48	0.1	1	-	-	-	-	-	2	-	1.00±0.57	0.010±0.005
		1	1	-	-	-	-	-	5	-	2.00±0.65	0.020±0.008
		10	-	-	-	-	-	-	2	-	0.67±0.47	0.007±0.004
		100	-	1	-	-	-	-	1	-	0.67±0.47	0.007±0.004
MoS_2 MP_S	48	0.1	1	1	-	-	-	-	-	-	0.67±0.47	0.007±0.004
		1	3	-	-	-	-	-	-	-	1.00±0.57	0.010±0.005
		10	-	-	-	-	-	-	1	-	0.33±0.33	0.003±0.003
		100	1	-	-	-	-	-	-	-	0.33±0.33	0.003±0.003

ctb= chromatid break, csb= chromosome break, f= fragment, dic= dicentric chromosome, scu= sister chromatid union, ex= chromatid exchange, p= polyploidy, en= endoreduplication, SE= standard error, PC (MMC)= positive control- mitomycin C, NC= Negative control, ***Significantly different from the negative control P<0.001 (z test).

The most common type of abnormality in MoO_3-treated ('3' was made a subscript) cells was polyploidy, followed by chromatid break, fragment, and endoreduplication. In the MoS_2 treatment, polyploidy was the most common abnormality, followed by chromatid break, chromosome break, and chromatid exchange = endoreduplication.

3.4. CBMN-Cyt Assay Results of NPs and MPs of MoO_3 and MoS_2

In this study, while the NPs and MPs of MoO_3 slightly increased micronucleus frequency in human lymphocytes, none was significant compared to the negative control (Figure 7). On the contrary, all the concentrations of MoS_2 NPs (except 0.1 µg/mL) significantly increased the micronucleus frequency over the control value (Figure 8). This increase was strongly concentration-dependent(r=0.84). MoS_2 MPs also increased the frequency of micronucleus, but only two of them (1 and 10 µg/mL) were significant and weakly concentration-dependent (r=0.53) compared to the negative control. Regarding nuclear bud, neither MoO_3 NPs and MPs nor MoS_2 NPs and MPs increased the frequency. None of these particles generated nucleoplasmic bridge (except MoS_2 NPs at 100 µg/mL, 48 h; was not significant) either. In our study, the nuclear division index and CBPI were not significantly affected by MoO_3 NPs and MPs or MoS_2 NPs and MPs. Either of these particles did not significantly change the frequency of cytostasis.

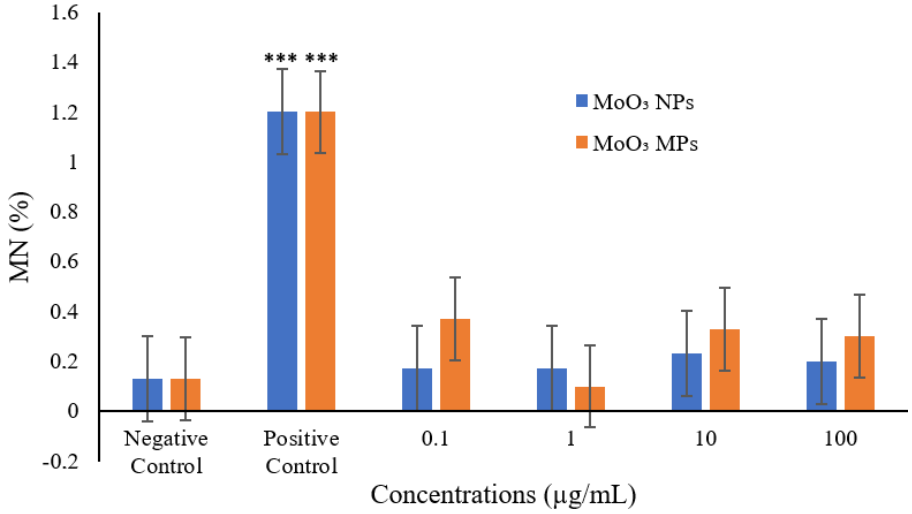

Figure 7. The frequency of MN in human lymphocytes exposed to MoO_3 NPs and MPs for 48 h.

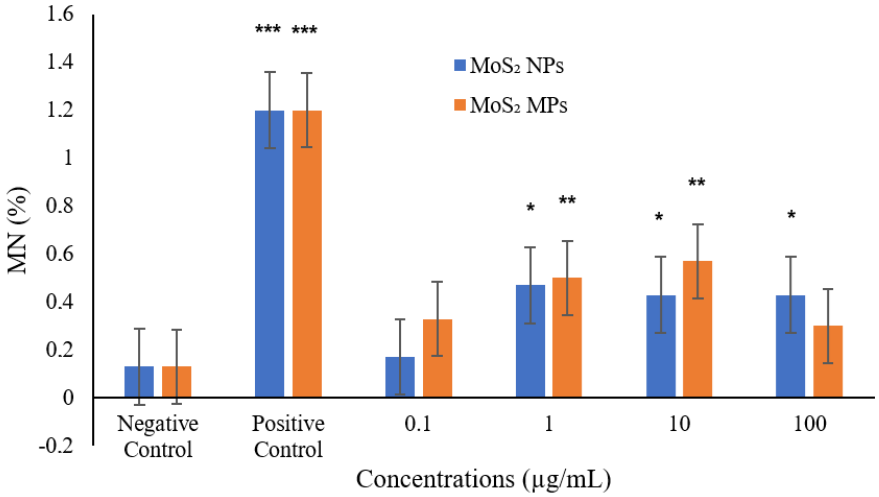

Figure 8. The frequecny of MN in human lymphocytes exposed to MoS_2 NPs and MPs for 48-h. *Significantly different from the control P<0.05 (z test). **Significantly different from the control P<0.01 (z test). ***Significantly different from the control P<0.001(z test). (Capitalize the letter 's' in the word 'Significantly')

3.5. Comet Assay Results of NPs and MPs of MoO_3 and MoS_2

In this investigation, both NPs and MPs of MoO_3 and MoS_2 significantly increased the tail length, tail intensity, and tail moment at all concentrations in isolated human lymphocytes compared to the negative control at both 1 and 3 h treatments (except the tail intensity at 0.1 µg/mL for MoS_2 MPs at 3 h treatment) (Tables 4 and 5). These increases were observed in tail length, tail density and tail moment for MoO_3 NPs (r=0.75, r=0.68 and r=0.68, respectively), MoO_3 MPs (r=0.21, r=0.50 and r=0.22, respectively), MoS_2 NPs (r=0.24, r=0.44 and r=0.27,

respectively) and MoS_2 MPs (r=0.42, r=0.43 and r=0.49, respectively) during 1 h of treatment. (Added sentence with red mark instead of 'These increases were concentration-dependent for tail length, tail intensity and tail moment at 1-h treatment for MoO_3 NPs (r=0.75, r=0.68 and r=0.68, respectively), MoO_3 MPs (r=0.21, r=0.50 and r=0.22, respectively), MoS_2 NPs (r=0.24, r=0.44 and r=0.27, respectively), and MoS_2 MPs (r=0.42, r=0.43 and r=0.49, respectively)' . At 3-h treatments, all the particles increased DNA damage concentration-dependently ('concentration-dependently' will be removed) in terms of tail length, tail intensity, and tail moment as follows; r=0.93, r=0.77 and r=0.77, respectively, for MoO_3 NP, r=0.69, r=0.55 and r=0.58, respectively, for MoO_3 MPs, r=0.58, r=0.52 and r=0.39, respectively, for MoS_2 NPs and r=0.70, r=0.43 and r=0.57, respectively, for MoS_2 MPs. Cell viability at 1- and 3-h treatments in isolated lymphocytes was determined as ≥ 80% and 87% for MoO_3 NPs, ≥ 75% and 89% for MoO_3 MPs, ≥ 75% and 80% for MoS_2 NPs, and ≥ 76% and 75% for MoS_2 MPs by trypan blue exclusion test, respectively.

Table 4. Effects of NPs and MPs of MoO_3 on DNA damage in human lymphocytes

Test substance	Treatment		Tail Length (μm)	Tail Intensity (%)	Tail Moment
	Time (h)	Concentration (μg/mL)			
NC	1	0.00	45.10±0.56	5.27±0.61	1.23±0.18
PC (H_2O_2)	1	100 μM	154.36±5.53*	30.24±1.38*	17.02±1.30*
MoO_3 NPs	1	0.1	83.02±2.99*	19.00±1.55*	7.34±0.84*
		1	86.55±2.68*	13.55±1.10*	4.33±0.52*
		10	105.32±4.40*	17.26±1.49*	7.96±0.96*
		100	86.42±3.42*	18.36±1.31*	6.87±0.94*
MoO_3 MPs	1	0.1	94.96±4.32*	21.71±1.48*	9.84±0.99*
		1	100.79±4.59*	19.04±1.26*	8.33±0.76*
		10	71.73±2.96*	19.50±1.21*	6.50±0.79*
		100	72.07±2.56*	16.71±1.07*	5.16±0.52*
NC	3	0.00	55.20±0.90	9.25±0.86	2.11±0.22
PC (H_2O_2)	3	100 μM	126.63±4.80*	23.56±1.29*	9.67±0.66*
MoO_3 NPS	3	0.1	55.20±0.90*	15.09±1.26*	5.88±0.93*
		1	68.11±2.44*	13.97±1.15*	4.51±0.53*
		10	70.73±2.88*	14.35±1.36*	6.26±1.00*
		100	139.06±6.13*	47.84±1.95*	32.64±2.27*
MoO_3 MPS	3	0.1	78.96±3.71*	14.38±1.13*	5.53±0.82*
		1	72.71±3.56*	13.81±1.18*	5.91±0.92*
		10	79.13±3.47*	13.90±1.20*	5.62±0.87*
		100	75.26±2.61*	13.13±1.11*	4.92±0.72*

NC= negative control, PC (H_2O_2)= positive control- H_2O_2, *significantly different from the negative control P<0.05 (t-test)

Table 5. Effects of NPS and MPs of MoS_2 on DNA damage in human lymphocytes

Test substance	Treatment		Tail Length (μm)	Tail Intensity (%)	Tail Moment
	Time (h)	Concentration (μg/mL)			
NC	1	0.00	45.10±0.56	5.27±0.61	1.23±0.18
PC (H_2O_2)	1	100 μM	154.36±5.53*	30.24±1.38*	17.02±1.30*
MoS_2 NPS	1	0.1	128.58±6.68*	25.15±1.62*	13.22±1.08*
		1	129.12±6.29*	22.51±1.37*	12.55±1.04*
		10	116.57±5.59*	23.66±1.62*	11.97±1.19*
		100	79.42±3.23*	18.37±1.24*	6.25±0.68*
MoS_2 MPS	1	0.1	65.85±2.24*	11.61±1.04*	3.55±0.48*
		1	128,87±5.72*	23.18±1.53*	11.32±1.04*
		10	100.61±5.82*	19.77±1.46*	12.29±1.74*
		100	70.68±3.47*	11.09±1.06*	4.48±0.75*
NC	3	0.00	55.20±0.90	9.25±0.86	2.11±0.22
PC (H_2O_2)	3	100 μM	126.63±4.80*	23.56±1.29*	9.67±0.66*
MoS_2 NPS	3	0.1	77.62±3.10*	13.43±1.13*	4.80±0.66*
		1	74.52±2.54*	14.39±1.07*	4.67±0.60*
		10	67.20±2.11*	12.23±1.15*	4.34±0.62*
		100	66.28±1.66*	13.09±1.08*	3.70±0.44*
MoS_2 MPS	3	0.1	72.83±3.22*	9.51±1.03	3.34±0.55*
		1	68.86±2.72*	15.72±1.36*	5.89±0.79*
		10	66.13±2.31*	11.88±0.94*	3.46±0.48*
		100	73.95±3.71*	11.57±0.96*	4.61±0.91*

NC= negative control, PC (H_2O_2)= positive control-H_2O_2, *significantly different from the negative control P<0.05 (t-test).

4. Discussion

The most critical features influencing nanomaterials interaction with cells and cellular components are morphology, size, size distribution, hydrodynamic diameter, polydispersity index, and surface chemistry (Murdock et al., 2008). Therefore, TEM, SEM, and DLS measurements were made in the present study. These sizes, assessed through electron microscopy, exceeded the manufacturer's specification of 10-80 nm for MoO_3 NPs and 100 nm for MoS_2 NPs due to the presence of extended 2D structures, resulting in larger particle sizes (Figures 1A-1F and Table 1) (Santos et al., 2023). Likewise, the average length/diameter measured for MoO_3 and MoS_2 MPs was deviated from the manufacturer's stated average size of 44 µm (325 mesh) (Table 1). There is a difference in shape and structure between the manufacturer and our results.

Regarding toxicity, various results were obtained in studies depending on size/shape. Disk-shaped MoS_2 NP (size 97 ± 32 nm and thickness equal to 8.5 nm ± 1.5 nm) and hexagonal-shaped micro-MoS_2 (size 1.92 ± 0.64 µm and thickness equal to 0.27 ± 0.15 µm) did not cause toxic effects in human hepatoma HepG2 cell line. After treating cells with MoS_2, the diameter of cells with particle clusters reached 300-400 µm on day 4. It was suggested that the lack of toxic effect was due to the lack of cell membrane disruption (Sobańska et al., 2020a). In a study, while bulk MoS_2 (> 2 µm) induced DNA damage in soil organisms, 2D MoS_2 NPs (90 nm) induced less damage to the DNA integrity, and it was observed that toxicity decreased as the size decreased. It has been suggested that these results are probably due to 2D MoS_2 NPs remaining particulate and retard ion leakage. This hypothesis suggests that 2D MoS_2 NP genotoxicity is primarily due to ion leaching rather than the particles themselves (Santos et al., 2023). MoS_2 showed more toxic effects in our study than MoO_3. Therefore, it can be argued that size indirectly affects toxicity.

DLS is an important technique widely used to determine particle size, size distribution, polydispersity index, and surface charge of small particles in suspension as simple, easy, and reproducible technique (Bhattacharjee, 2016). In our study, the electron microscopy measurement values of MoO_3 NPs and MoS_2 NPs were larger than the observed HD measurement (Table 1 and Figure 2). The hydrodynamic diameter, which is determined using the DLS approach, is related to the particle's movement in the plate's thickness, width, and length in all three directions. Consequently, the hydrodynamic diameter is ultimately determined by the thickness of a single particle, which resulted in a decrease in comparison with the size determined by electron microscope observations (Sobańska et al., 2020b). This study showed that the polydispersity index for both MoO_3 NPs (0.704) and MoS_2 NPs (0.958) had a wide particle size distribution, confirming the presence of agglomerates. The study by Singh et al. (2024) yielded considerable variation in both the effective diameter (HD) and polydispersity index (PI) of MoS_2 nanosheets (trigonal prismatic) depending on the dispersion medium employed. In RPMI medium, HD was 549.08 ± 41.15 nm to 6959.12 ± 7185.11 nm and PDI was 0.17 ± 0.07 to 1.77 ± 2.49, while in FBS (20 % v/v) + RPMI medium HD was 197.30 ±31.43 nm to 262.94 ± 5.92 nm and PDI 0.17 ± 0.03 to 0.37 ± 0.07. After 48 and 72 hours, the abrupt decrease observed in these values indicates that MoS_2 nanosheets precipitated in the medium. The addition of 500 mg/L of MoS_2 to a culture containing RPMI resulted in a reduction in cell viability in both HepG2 and HL-60 cells over 48 h. These situations may be due to the aggregation of nanosheets in RPMI medium. It has been reported that the significant change in the effective diameter and polydispersity index of MoS_2 dispersed in RPMI can be attributed to the high ionic strength of the medium and may be affected by interactions with biomolecules in environmental matrices, serum, etc (Singh et al. (2024).

Zeta potential is another chemical property that exhibits the electrochemical equilibrium at the particle-liquid interface and provides information about the particle's surface charge (Lunardi et al., 2021). The electrostatic stability of a suspension is typically regarded as adequate when the absolute value of the ζ-potential is 30 mV or greater. Particles having zeta potentials between ±10 and ±30 mV reveal incipient instability, while between ±0 and ±10 mV show rapid coagulation or flocculation (Clogston et al., 2011; Kaur et al., 2021; Lunardi et al., 2021). We applied ultrasonication to all suspensions to prevent agglomeration and disperse particles into single nanoparticles. However, the NPs tend to agglomerate over time because of interparticle adhesion forces. Positively charged NPs have been reported to provide higher interaction strength with cells than negatively charged particles and cationic particles generally exhibit more significant toxicity associated with the disruption of cell walls (Clogston et al., 2011; Shao et al., 2015). DLS measurements the negative zeta potential was 34.5 ± 9.91 mV for MoO_3 NPs, 16.1± 4.32 mV for MoO_3 MPs, 27.9± 7.18 mV for MoS_2 NPs and 14.2± 5.94 mV for MoS_2 MPs (Table 2). Zeta potential between -30 and +30 mV may cause agglomeration and affect cell membrane interaction (Clogston et al., 2011; Kaur et al., 2021; Lunardi et al., 2021).

MI, NDI, CPBI, and % cytostasis were assessed in human lymphocytes to investigate the cytotoxic effects of both MoO_3 and MoS_2. MI measures the proportion of cells undergoing mitosis (Akbas et al., 2022). The present study demonstrated that most concentrations of MoO_3 NPs, MoO_3 MPs, and MoS_2 NPs exhibited cytotoxic effects. Conversely, only the lowest and highest concentrations of MoS_2 MPs showed such effects. Although there are slight differences between the cytotoxic effects of particles, the order of toxic effect is as follows: MoO_3 MPs> MoS_2 NPs> MoO_3 NP> MoS_2 MPs. This reveals that NPs are not always more cytotoxic compared to MPs. In this investigation, none of the NPs and MPs significantly affected NDI, CBPI,

and % cytostasis compared to the negative control. Kumari and Mangala (2022) determined that the MoO_3 NPs (30-47 nm) (78.64 µg/mL) and MPs (190.23 µg/mL) decreased cell viability by 50% in MCF7-human breast adenocarcinoma cells at 24-h application. MoO_3 NPs, at 0.4 mg/mL concentration, were also found to have cytotoxic effects on invasive breast cancer cell line iMCF-7, induced apoptosis, and generated reactive oxygen species (Anh Tran et al. 2014). Sahoo et al. (2022) demonstrated that MoS_2 NPs (hexagonal; 2-10 nm; 5, 10, and 20 µg/mL; 24 h) elicited a dose-dependent increase in ROS formation and a concomitant decrease in cell viability, ultimately resulting in a cytotoxic effect at high concentrations. Our results revealed that the test substances investigated decreased the mitotic index, which was in accordance with some of the previous studies. The decrease in the mitotic index may be due to the cell cycle inhibition, induction of mitochondria-dependent apoptosis, and ROS production or zeta potential value and agglomeration behavior of MoO_3 and MoS_2 (Terpilowska et al., 2018; Li et al., 2021; Libalova et al., 2024). On the other hand, increasing the mitotic index might be due to the increasing effect of test substances on cell viability by scavenging ROS and reducing inflammation at different concentrations and application periods (Decker et al., 2021; Duan et al., 2022). For example, Chen et al. (2018) developed a nanozymatic antioxidant system with few-layer MoS_2 nanotubes that scavenged ROS in Escherichia coli, Staphylococcus aureus, and A549 cells in vivo. Moreover, MoS_2 nanosheets showed superior protection against H_2O_2-induced oxidative damage with peroxidase-like activity by transferring electrons instead of ROS production with its enzyme feature. This can be attributed to Mo^{4+}/Mo^{6+} oxidation on the surface of MoS_2 nanosheets.

The genotoxicity of a chemical can be determined from variations in cellular behavior and examination of damage generated to DNA and chromosomes. No single genotoxicity assay can compare, rank, and evaluate the genotoxic potential for all ENMs currently available and used for various purposes. Therefore, in this study, we applied three genotoxicity tests to obtain whether MoO_3 and MoS_2 NPs and MPs generate damage in human lymphocyte cells: chromosome aberration, cytokinesis block micronucleus, and comet tests. One of them, the chromosome aberration test, is used to determine agents that produce structural and numerical chromosomal abnormalities resulting from the treatment with genotoxic chemicals (Mamur et al., 2022; Santibáñez-Andrade et al., 2022). CAs comprise structural and numerical abnormalities, resulting in genomic instability. Structural aberrations, either chromatid or chromosome, may result from chemicals' clastogenic effects (DNA damage). Deletions are the most common, followed by amplification and then unbalanced translocations. Numerical abnormalities primarily comprise aneuploidy and chromosome instability (CIN), represented by chromosome gain or loss. Both types of CAs are reported to be the reason for various genetic and non-communicable diseases. There is also considerable evidence that chromosomal aberrations and associated events triggering modifications in oncogenes and tumor suppressor genes of somatic cells are connected to cancer production in humans and experimental animals (Rossner et al., 2005; Santovito et al., 2014; Vodenkova et al., 2015; Raj et al., 2023).

While NPs and MPs did not cause significant chromosome abnormalities, some structural and numerical chromosome abnormalities were observed. These damages may originate from non-repair or misrepair of DNA double-strand breaks, mismatches between two breaks along the length of the chromosome, and insufficient activation of the G2 checkpoint in cells with a markedly reduced G2 arrest (Helleday et al., 2007; Zeng et al., 2023). Polyploidy may result from increased genome DNA content (Frawley and Orr-Weaver, 2015). Endoreduplication arises if DNA replication occurs without mitosis (Jiang et al., 2022). When DNA damage occurs, the cell cycle checkpoints detect this damage and arrest G1, DNA synthesis, and G2/M transition until various repair mechanisms repair the damage. The activation of the checkpoint prevents mitotic entry of the damaged cells. If damages cannot be repaired or are defectively repaired, this may lead to p53-dependent apoptosis (Zeng et al., 2023; Libalova et al., 2024). Defective DNA damage repair or defects of DNA damage checkpoints generate genomic instability and rapid aging and predispose the organism to neurological disorders, immunodeficiency, and cancer progression (Santovito et al., 2014; Vodenkova et al., 2015; Raj et al., 2023).

In the literature, both negative and positive findings of molybdenum and molybdenum species have been reported for mutations in bacterial and mammalian cells. For example, Burzlaff et al. (2017) reported that sodium molybdate dihydrate (1.6-5000 mg/mL) did not induce reverse mutations in five Salmonella typhimurium strains (TA98, TA100, TA1535, TA1537 and TA102) and mutagenic or clastogenic effects in the tk locus of L5178Y mouse lymphoma cells (1000-2060 mg/mL). It did not generate clastogenic or aneugenic effects in micronucleus test in human lymphocytes. Due to their negative results and all species release the molybdate ion $(MoO_4)_2$ under morphological conditions, authors suggested that their results can be read across to other molybdenum species; no evidence of genotoxicity of molybdenum species (Burzlaff et al. 2017). The absence of mutagenic potential was also demonstrated in TA98 and TA100 strains of Salmonella typhimurium for sodium (Burzlaff et al., 2017) and potassium molybdate (Nishioka, 1975). Calcium molybdate ($CaMoO_4$) NPs (spherical; 50-250 nm, forming some agglomerates of mesostructures with size ~6 µm) synthesized by Nobre et al. (2020) did not affect the survival rate between 1.5625 and 100 mM and did not induce a genotoxic effect at the investigated concentrations (6.25, 25.0, and 100.0 mM) in Drosophila melanogaster. Authors suggested that calcium molybdate nanocrystals could not interact with the DNA and did not

induce point mutations, breaks, deletions, or mitotic recombination (Nobre et al., 2020). In Daphnia magna, a microcrustacean sensitive enough to evaluate the toxicity of the various compounds, sodium molybdate (LC50 value at 48 h was 2847.5 mg/L) did not reveal toxic or genotoxic effects either (Diamantino et al., 2000). Moreover, Duan et al. (2022) reported excellent scavenging properties of Mo against H_2O_2, $\cdot O_2$- and ·OH ROS species by catalyzing redox and oxygen-transfer reactions (Chen et al., 2018; Duan et al., 2022).

Contrary to the previous observations, Ladon et al. (2004) determined in patients who underwent metal hip arthroplasty that high molybdenum concentration had a higher rate of chromosomal translocations than patients with low molybdenum concentration at 6th, 12th, and 24th months after surgery. Daley et al. (2004) have revealed that the molybdenum concentration in wear debris removed from the body was associated with the total micronucleus index, both centromere-positive and centromere-negative (indicating chromosomal breakage and aneuploidy, respectively) in tissue culture. Increased frequencies of chromosomal aberrations in peripheral blood lymphocytes have been reported to occur when workers are exposed to molybdenum, molybdenite and molybdenum trioxide (Babayan et al., 1980). Terpilowska and Siwicki (2018) showed that MoO_3 stimulated significant chromosome abnormalities in BALB/3T3 and HepG2 cells between 100 and 1400 µM. Furthermore, an increase in the number of reverse mutations with or without metabolic activation was detected. Cui et al. (2023) reported that excessive molybdenum (5, 10, 20, and 50 mg/kg BW/day) induced apoptosis-related DNA damage in splenocytes and thymocytes and caused apoptosis of lymphocytes in sheep. The toxic effects of two-dimensional molybdenum disulfide nanomaterials on *Eisenia fetida* were reported by Sun and colleagues (2023). While surface perfect MoS_2 (1.79±0.07 nm) produced an increase in the level of reactiveoxygen species (ROS) and a decrease in the activity of the mitochondrial respiratory electron transport chain III complex, surface-defective MoS_2 (1.91±0.27 nm) triggered a more severe ROS increase and apoptosis with depolarization of the mitochondrial membrane potential. Therefore, researchers have reported that the role of surface defects resulting from synthesis or accumulated from environmental effects should be considered when evaluating the toxicity of 2D materials (Sun et al., 2023). Wang et al. (2016) evaluated acute toxicity of various salts from Mo to *D. magna* following 48 h of treatment and observed that toxicity elevated in the following order: sodium molybdate ($Na_2MoO_4 \cdot 2H_2O$) < molybdenum trioxide (MoO_3)< ammonium molybdate (NH4)6Mo7O24.4H2O), in solution. The authors report that the toxic effect of molybdenum in the aquatic system depends largely on the form of molybdenum salts used. However, they concluded that the toxicity of molybdenum is also linked to the influence of background water quality. High concentrations of molybdenum have been reported to be toxic effective to many organisms, including mammals and freshwater invertebrates (Khangarot, 1991). In addition, the toxic effect of molybdenum has been also reported to depend on the contribution of associated conjugate cations (Wang et al., 2016).

While our study's result coincided with some of the experiments in the literature, it was not coincident with others. Our results indicated that while MoO_3 and MoS_2 did not significantly increase the frequency of aberrant cells and CAs/Cell, they caused a significant decrease in the mitotic index. The significant reductions in the mitotic index might be due to the toxic or genotoxic effects of these NPs, therefore, a decrease in the proportion of cells, cells undergoing mitosis, or an increase in the number of cells encountering apoptosis due to unrepairable damages in DNA, chromosome or cell cycle checkpoints (Nobre et al., 2020; Li et al., 2021; Santibáñez-Andrade et al., 2022; Libalova et al., 2024; Singh et al., 2024). The lack of a significant increase in CAs frequency may be due to the scavenging of ROS by Mo showing nanozyme properties; DNA repair mechanisms repaired the damages in cells that were not directed apoptosis, controlled cell death. In our study, MoO_3 and MoS_2 have negative zeta potential and have shown agglomeration potential. These physicochemical properties may have caused the test substances not to interact strongly with DNA (Nobre et al., 2020). As a result, variations in toxicity of Mo species may be due to the size, shape, and other physicochemical properties, different compounds in that substance, the difference in the synthesis protocol, the difference in the cell types treated, and behavior in culture media of particles (Uboldi et al., 2016; Sikder et al., 2020; Vazquez-Muñoz et al., 2020; Sun et al., 2023).

CBMN-Cyt is an extensively used test to assess cytotoxic, clastogenic (DNA and chromosome damage), aneugenic (principally affects non-DNA targets like spindle fibers and kinetochore and disturbs the cell division cycle), and cytostatic effects generated by genotoxic agents (Fenech et al., 2020; Farabaugh et al., 2023; Raj et al., 2023). It is a comprehensive, accurate, and well-established method that is especially used with comet assay to evaluate the genotoxic effects of nanomaterials. Genomic instability, such as micronuclei (MNi), nucleoplasmic bridges (NPBs), and nuclear buds (NBUDs), can be evaluated by this assay. MNi are formed from whole chromosomes or chromosome fragments that do not correctly segregate to the poles of the cell in mitosis. NPBs are produced from dicentric chromosomes triggered by telomere end-fusions, mis-repaired DNA breaks, or failure of complete chromatid separation. Nuclear bud represent the procedure of exclusion of amplified DNA, DNA repair complexes, and probably extra chromosomes from aneuploid cells (Fenech et al., 2020; Mamur et al., 2022; Struys et al., 2023). In this study, while the NPs (except 0.1 µg/mL) and MPs (1 and 10 µg/mL) of MoS_2 significantly increased micronucleus frequency in human lymphocytes, none the NPs and MPs of MoO_3 was increased significant compared to the negative control. NDI, NPB, NBUD, CBPI and CBPI showed that the results were not significantly affected by MoO_3 NPs and MPs or

MoS_2 NPs and MPs. NDI is an index of cellular mitotic division that oddly elevates or decreases in line with the proliferative capability of the cell. CBPI displays the cytotoxic effects resulting from the exposure of chemical agents. Cytostasis is used for chemicals that inhibit cellular growth and division (Lorge et al., 2008; Nefic and Handzic, 2013; Rodrigues et al., 2018). Investigations unveiled both positive and negative results for MoO_3 and MoS_2 particles. Gibson et al. (1997) reported that molybdenum trioxide (250, 500, and 750 mg/mL) revealed a positive effect in Syrian Hamster Embryo (SHE) cells in micronucleus and cell transformation assay when applied for 24 h. Titenko-Holland et al. (1998) evaluated ammonium molybdate [(NH4)6 Mo7O24r4H2O] and sodium molybdate [(Na2MoO4rH2O)] (0.1, 0.5, 1 and 5 mM) using three genotoxicity assays; micronucleus in human lymphocytes *in vitro* and in mouse *in vivo* and dominant lethal assay in mice. All three tests revealed positive evidence of modest genotoxicity for molybdenum salts, especially at relatively high concentrations, both *in vitro* and *in vivo*. Ammonium molybdate was more effective than sodium molybdate, induced a dose-dependent decrease in cell viability and replicative index, as well as an increase in micronucleus formation in binucleated lymphocytes. Significant dose effect was determined for both chemicals for centromere positive MN and negative MN. Therefore, the authors suggested that the most probable mechanism of molybdenum genotoxicity involves chromosome lagging, resulting in aneuploidy and chromosome breakage (Titenko-Holland et al., 1998). In contrast, using the MN test, Burzlaff et al. (2017) did not determine clastogenic or aneugenic effects following sodium molybdate dihydrate exposure of cultured lymphocytes. In CHO-K1 cells, MoS_2 NPs (138±52 nm; 0, 0.05, 0.5, 5, 20, and 50 µg/mL) have no toxic effect at low doses (0.5 and 5 µg/mL), but the number of cells per field decreased at the highest concentration tested (50 µg/mL). While shaking the culture medium contributed to agglomerate reduction in size and number, these NPs did not affect the MN formation. Therefore, sodium molybdate dihydrate was reported to have non-genotoxic effects (García-Carpintero et al., 2023). Moreover, MoO_{3-X} nanodots were reported tohave excellent ROS scavenging capacity (Duan et al., 2022). In Chinese hamster ovary (CHO) cells exposed to molybdenum trioxide, there was no increase in either chromosome aberrations or SCEs with or without metabolic activation [NTP, 1997; NTP (National Toxicology Program) (1997). Such discrepancies might result from the shape, size, size distribution, hydrodynamic diameter, zeta potential, agglomeration, concentrations, and treatment periods. Interspecies variations in sensitivity to molybdenum and variations in sensitivity of short-term human lymphocytes in culture versus other tests might be other explanations (Titenko- Holland et al., 1998).

The comet assay, together with the CBMN-Cyt, is the most frequently applied test to determine the genotoxicity of NMs. The types of damage detected include DNA strand breaks, alkali labile regions, alkylated and oxidized nucleobases, DNA-DNA and DNA-protein cross-links, and DNA adducts. It also determines the repair of all the damages mentioned above at the individual cell level (Collins et al., 2023). The tail length, intensity (% tail DNA), and moment (the product of the tail length and the fraction of total DNA in the tail) are the most common parameters used as indicators of DNA damage caused by chemicals. Though some researchers select the tail moment as a common descriptor, % tail DNA is the most common parameter and reveals a linear correlation with DNA damage induced by chemicals, either by direct or indirect attacks on the DNA (Collins, 2004).

In this study, both NPs and MPs of MoO_3 and MoS_2 caused a significant increase in DNA damage in both 1 and 3 h treatment. In general, DNA damaging parameters were higher for both NPs and MPs at 1 h treatment compared to 3 h treatments, except for the highest concentration of MoO_3 NPs at 3 h treatment. The increase in tail length, tail intensity, and tail moment might have resulted from DNA damage that was not repaired. Decreasing DNA damage after 3 h treatment, on the other hand, may indicate the repairing process of damages or the death or apoptosis of heavily damaged cells (Duijf et al., 2019; Bankoglu et al., 2021; Tung and Gandhi, 2023).

While our results coincide with some of the previous studies, they differ from others. For example, Terpilowska et al. (2018) reported that 100-1400 µM MoO_3 (microelements-24 h) caused DNA damage in BALB/3T3 and HepG2 cells. In another experiment, Siddiqui et al. (2015) showed molybdenum NPs (40 nm) to induce significant induction of DNA damage in L929 mouse fibroblast cells in a concentration-dependent manner using the standard alkaline comet assay. The cells exposed to 10, 25, 50, and 100 µg/mL of Mo-NPs for 24 h revealed a 9.9-, 15-, 23.2-, and 27.7-fold increase in % tail DNA, respectively. In addition, significant production of oxidative stress verified by the increase in lipid peroxidation (LPO) and ROS generation, as well as the reduction in the antioxidant enzyme GSH and catalase levels, were determined. In the cell cycle analysis, NPs generated a significant G2/M arrest and an increase in apoptotic G2/M peak. Therefore, the authors proposed that oxidative stress may be the primary mechanism of toxicity, and ROS may be a crucial mediator of cell death induced by Mo-NPs.

Sobańska et al. (2020b) evaluated nanosized (97± 32 nm-disc-shaped) and micron-sized (1.92± 0.64 µm-lamellar shape and a layered structure) MoS_2 (dose of 1.5 or 5 mg/kg body weight) after single intratracheal instillation in rats. After exposure to both forms for 24 hours or 7 days, numerous macrophages containing particles were detected in the BALF cells isolated from animals; macrophages are much more for the microform of MoS_2. Inflammatory changes in the respiratory system were observed, which were slightly powerful for the micron-

sized form. However, the hematological and biochemical parameters revealed no statistically significant differences. In the comet assay, MoS_2 nano- and microparticles showed no increase in DNA damage over the control values (Sobańska et al., 2020b). In mice, Wang et al. (2015b) compared 2D MoS_2 NPs with the aggregated MoS_2 and observed that the nanoform generated a lower inflammatory response than the microsized aggregated MoS_2. As a photothermal therapy agent, MoS_2 nanosheets and nanoplates coated with poly(ethylene glycol) (PEG) were found nontoxic for Balb/c mice, but they revealed anti-tumor abilities when combined with infrared irradiation (Wang et al., 2015a). MoO_3 NPs at prolonged exposure caused an increase in the level of release of interleukin 6, DNA damage, and cell death (Božinović et al., 2020). MoS_2 has been observed to cause increased genotoxicity in mouse lungs at moderate and high exposures (Sørli et al., 2023).

In *Oryza sativa* (*('Oryza sativa'* has been italicized) seedlings, molybdenum trioxide (MoO_3) ('3' was made a subscript) exposure at 100, 500, and 1000 ppm doses induced a gradual reduction in root and shoot lengths (Sharma et al., 2021). In *Allium cepa ('Allium cepa'* has been italicized), sodium molybdate dihydrate (1000, 2000, and 4000 mg/L; 72 h) induced a significant and dose-dependent decrease in physiological (germination percent, root length, and weight gain) parameters, while a significant increase was observed in biochemical (free proline content, MDA, SOD, and CAT enzyme activity) features. In addition, it caused a significant increase in MN frequency, chromosomal aberrations, and anatomical damage dose-dependently. In the comet assay, increasing DNA damage was correlated with increasing molybdenum dose. This molybdenum compound caused a significant and dose-dependent decrease in mitotic index. The decline determined in physiological parameters as a result of excessive molybdenum treatment was clarified by the fact that molybdenum inhibits micro and macro element uptake by *A. cepa ('Allium cepa'* has been italicized) roots, generates damage to the anatomical construction of the roots, and decreases the mitotic division of root cells (Özkan et al., 2024). In the literature, investigations revealed that high quantities of trace elements, such as copper, create physiological toxicity and prevent the uptake of water and nutrients (Kalefetoğlu Macar et al., 2020), damage the physiological structure of plants by causing a decrease in starch, sugar, protein, and nitrogen contents (Gopal et al., 2016). As a result, it hinders cell division in plant root tips and decreases root elongation (Macar et al., 2020). In our study, we observed a significantly reduced mitotic index for both molybdenum NPs and MPs following 24- and 48- hour exposure in human lymphocytes. Decreasing was more prominent, especially at higher concentrations. Although there was a significant increase in DNA damage in comet assay following 1- and 3-h treatments, these particles did not increase the frequency of chromosome aberrations. While MoO_3 particles induced no MN formation, some concentrations of MoS_2 particles generated significant MN formation. To investigate some discrepancies and the timewise variations of induction and reduction of DNA damage, TK6 cells were treated with one concentration (60 μM) of the oxidizing and highly reactive substance hydrogen peroxide (H_2O_2). The alkaline comet assay was applied with the treated cells and the solvent controls after 0.5, 1, 2, 3, 4, 5, 6, and 20 h. H_2O_2 exposure drives its maximum damage after 0.5 h; the damage decreased to about half within an hour, and the DNA strand breaks decreased progressively over time, reaching the control level after 20 h (Bankoglu et al. (2021). In HeLa cells, Duthie and Collins (1997) measured the DNA repair activity up to an hour following 30 min H_2O_2 treatment on ice. They reported a quick repair of H_2O_2-induced damage, which almost completely reduced within an hour after the treatment. In HepG2 cells treated with H_2O_2 for 5 min, 30 min, 40 min, 1 h, and 24 h, a significant increase in DNA damage after 5 min, which reached its maximum at 1 h was determined. However, there was no significant difference in DNA damage after 24 hours compared to control (Benhusein et al., 2010). Ngo et al. (2021) reported that halftime for the repair of H_2O_2-induced DNA damage in the comet assay was 24 min for TK6 cells and 39 min for a human lymphocyte. DNA damages we observed might be interpreted in such a way that MoO_3 and MoS_2 NPs and MPs can interact with DNA and induce damage following 1- and 3-h of exposure, but most or some of these damages might be repaired after 24-h of exposure because we did not observe any significant increase in CAs following 24- and 48-h treatment. Similarly, DNA damage was not significant in long-term treatment (24 h and 7 days), possibly due to the repair of DNA damage or death of damaged cells during long-term treatment, compared to control (Sobańska et al., 2020b). On the other hand, the reduction in the mitotic index may show an inhibitory effect of molybdenum in terms of micro and macro element uptake by human cells and then a decrease in the mitotic division. This may also result from the activation of the DNA repair process with an obvious cell cycle arrest in the G2/M phase in damaged cells or cell death/apoptosis of heavily damaged cells induced by these particles (Siddiqui et al., 2015; Bankoglu et al., 2021; Singh et al., 2024).

The genotoxic mechanisms of NPs are still not fully understood. However, based on the data obtained, it is stated that exposure to NPs can be genotoxic in living things and cells in two critical ways: primary and/or secondary (Magdolenova et al., 2014). Primary genotoxicity refers to ROS-mediated DNA damage without inflammation and direct physical interaction between particles and genomic DNA (Schins and Knaapen, 2007; Saber et al., 2015). Secondary genotoxicity implies that DNA damage results from the effects of reactive oxygen species and reactive nitrogen species (RNT), particle-induced inflammation, and other secondary mediators

(cytokines, chemokines) that occur during the acute response. NPs entering the cell induce microglia activation, ROS production, and activation of signaling pathways in inflammation, affecting the central nervous system and immune cells through proinflammatory response and genotoxicity (Joo and Zhao, 2017).

4. Conclusion

Our results demonstrated that neither MoO_3 nor MoS_2 increased the frequency of CAs and CAs/Cell. Only MoS_2 caused a significant increase in MN frequency. Both MoO_3 and MoS_2 displayed a significant decrease in the mitotic index. Comet assay results showed that both NPs and MPs of MoO_3 and MoS_2 increased the DNA damage. The reduction in mitotic index may be due to DNA damage causing apoptosis or mitotic inhibition. Decreased mitotic index, increased MN frequency, and DNA damage may be caused by oxidative stress. The decrease in the mitotic index may be caused by DNA damage or oxidative stress- inducing mitotic inhibition or apoptosis. Apoptosis may also be why no significant abnormalities were observed in the CAs assay (Sun et al., 2023). With comet assay, we evaluated the effects of short-term exposure in isolated lymphocytes. CAs and CBMN-Cyt assay determined the effects of long-term exposure in cultured lymphocytes. While DNA damage was observed in the comet test, the abnormality frequency did not increase in the CAs test. These results may be due to the repair of DNA damage or the death of damaged cells in the CAs test. While MoO_3 NPs and MPs did not cause significant abnormalities in the CAs and MN tests, MoS_2 NPs and MPs caused significant abnormalities in MN. No abnormality in treatment with MoO_3 NPs and MPs may have been observed due to DNA damage repair or scavenging ROS through catalyzing redox and oxygen-transfer reactions of Mo or apoptosis (Duan et al., 2022; Singh et al., 2024). We observed that the size of both NPs and MPs of MoO_3 and MoS_2 had no direct effect on toxicity. Negative zeta potential value and agglomeration potential may have played a role in the toxicity of both NPs and MPs of MoO_3 and MoS_2 (Nobre et al., 2020). In this study, potential genotoxic and cytotoxic effects of NPs and MPs of MoO_3 and MoS_2 used in bioimaging and cancer treatment were investigated for the first time on human lymphocytes *in vitro*. MoS_2 showed more toxic effects than MoO_3. Our results suggest that MoO_3 and MoS_2 may have weak genotoxic and cytotoxic effects. There are conflicting data in the literature regarding the genotoxic/cytotoxic effects of NPs and MPs (Decker et al., 2021; Kumari and Mangala, 2022; García-Carpintero et al., 2023; Sun et al., 2023). The contradictory results of MoO_3 and MoS_2 NPs on living organisms may be due to nanomaterials' different physical and chemical properties, concentrations, treatment periods, varying test species, and test systems. The differences in results available can be due to changes in the properties of NPs by the synthesis protocol used, coating, zeta potential, agglomeration, the presence of natural organic matter, behavior in culture media, and size and the difference in cell types (Uboldi et al., 2016; Sikder et al., 2020; Vazquez-Muñoz et al., 2020; Sun. et al., 2023; Singh et al., 2024). Therefore, these particles' toxicity potential and underlying mechanisms should be investigated in more detail.

Author Contributions

The percentages of the authors' contributions are presented below. The authors reviewed and approved the final version of the manuscript.

	N.K.	F.U.	E.A.	G.Ç.İ.	D.Y.
C	60	40	-	-	-
D	40	30	10	10	10
S	-	100	-	-	-
DCP	40	30	10	20	-
DAI	40	30	10	10	10
L	40	20	20	10	10
W	40	20	20	10	10
CR	30	40	10	10	10
SR	40	30	10	10	10

C=Concept, D= design, S= supervision, DCP= data collection and/or processing, DAI= data analysis and/or interpretation, L= literature search, W= writing, CR= critical review, SR= submission and revision.

Conflict of Interest

The authors declared that there is no conflict of interest.

Ethical Consideration

This research was approved by the Clinical Research Ethics Committee of the Faculty of Medicine at Gazi University (Date: 18/10/2021; No: 07; modified format 27/12/2021; No: 240).

Acknowledgements

This study is based on Nur Korkmaz's doctoral thesis. The supervisor of this thesis is Fatma Ünal.

References

Akbas E, Unal F, Yuzbasioglu D. 2022. Genotoxic effects of gadobutrol and gadoversetamide active substances used in magnetic resonance imaging in human peripheral lymphocytes in vitro. Drug Chem Toxicol, 45(6): 2471-2482.

Akhondipour M, Faghihi Zarandi A, Amirri A, Gommnami N, Vazirinejad R. 2018. Studying the toxicity of molybdenum trioxide nanoparticles in male Wister rats. J Occup Health Epidemiol, 7(4): 233-239.

Anh Tran T, Krishnamoorthy K, Song, YW, Cho SK, Kim SJ. 2014. Toxicity of nano molybdenum trioxide toward invasive breast cancer cells. ACS Appl Mater Interfaces, 6(4): 2980-2986.

Appel JH, Li DO, Podlevsky JD, Debnath A, Green AA, Wang QH, Chae J. 2016. Low cytotoxicity and genotoxicity of two-dimensional MoS2 and WS2. ACS Biomater Sci Eng, 2(3): 361-367.

Asadi F, Sadeghzadeh M, Jalilvand A, Nedaei K, Asadi Y, Heidari A. 2019. Effect of molybdenum trioxide nanoparticles on ovary function in female rats. J Adv Med Biomed Res, 27(121): 48-

53.

Babayan EA, Bagramyan SB, Pogosyan AS. 1980. Effect of some chemical hazards involved in molybdenum production on the chromosome apparatus of experimental animals and humans. Gig T Prof Zabol, 33-36.

Bakhoum SF, Cantley LC. 2018. The multifaceted role of chromosomal instability in cancer and its microenvironment. Cell, 174(6): 1347-1360.

Bankoglu EE, Schuele C, Stopper H. 2021. Cell survival after DNA damage in the comet assay. Arch Toxicol, 95(12): 3803-3813.

Benhusein G, Mutch E, Aburawi S, Williams F. 2010. Genotoxic effect induced by hydrogen peroxide in human hepatoma cells using comet assay. Libyan J Med, 5(1): 4637.

Bhattacharjee S. 2016. DLS and zeta potential–what they are and what they are not?. J Cont Release, 235: 337-351.

Božinović K, Nestić D, Centa UG, Ambriović-Ristov A, Dekanić A, de Bisschop L, Majhen D. 2020. In-vitro toxicity of molybdenum trioxide nanoparticles on human keratinocytes. Toxicology, 444: 152564.

Burzlaff A, Beevers C, Pearce H, Lloyd, Klipsch K. 2017. New studies on the in vitro genotoxicity of sodium molybdate and their impact on the overall assessment of the genotoxicity of molybdenum substances. Regul Toxicol Pharmacol, 86: 279-291.

Chen T, Zou H. Wu X, Liu C, Situ B, Zheng L, Yang G. 2018. Nanozymatic antioxidant system based on MoS2 nanosheets. ACS Appl Mater Interfaces, 10(15): 12453-12462.

Clogston JD, Patri AK. 2011. Zeta potential measurement. In: McNeil S, editors. Characterization of nanoparticles intended for drug delivery: Methods in molecular biology. Humana Press, Totowa, New Jersey, USA, pp: 63-70.

Collins A, Møller P, Gajski G, Vodenková S, Abdulwahed A, Anderson D, Azqueta A. 2023. Measuring DNA modifications with the comet assay: A compendium of protocols. Nat Protoc, 18(3): 929-989.

Collins AR. 2004. The comet assay for DNA damage and repair: principles, applications, and limitations. Mol Biotechnol, 26(3): 249-261.

Cui SG, Zhang YL, Guo HW, Zhou BH, Tian EJ, Zhao J, Wang HW. 2023. Molybdenum-induced apoptosis of splenocytes and thymocytes and changes of peripheral blood in sheep. Biol Trace Elem Res, 201: 1-11.

Daley B, Doherty AT, Fairman B, Case CP. 2004. Wear debris from hip or knee replacements causes chromosomal damage in human cells in tissue culture. J Bone Joint Surg Br, 86(4): 598-606.

Decker S, Kunisch E, Moghaddam A, Renkawitz T, Westhauser F. 2021. Molybdenum trioxide enhances viability, osteogenic differentiation and extracellular matrix formation of human bone marrow-derived mesenchymal stromal cells. J Trace Elem Med Biol, 68: 126827.

Desai ML, Jha S, Basu H, Saha S, Singhal RK, Kailasa SK. 2020. Simple hydrothermal approach for synthesis of fluorescent molybdenum disulfide quantum dots: Sensing of Cr^{3+} ('3+' made a superscript) ion and cellular imaging. Mater Sci Eng C, 111: 110778.

Diamantino TC, Guilhermino L, Almeida E, Soares AM. 2000. Toxicity of sodium molybdate and sodium dichromate to Daphnia magna Straus evaluated in acute, chronic, and acetylcholinesterase inhibition tests. Ecotoxicol Environ Saf, 45(3): 253-259.

Duan G, Wen L, Sun X, Wei Z, Duan R, Zeng J, Gao M. 2022. Healing diabetic ulcers with MoO3– X nanodots possessing intrinsic ROS-scavenging and bacteria-killing capacities. Small, 18(10): 2107137.

Duijf PH, Nanayakkara D, Nones K, Srihari S, Kalimutho M, Khanna KK. 2019. Mechanisms of genomic instability in breast cancer. Trends Mol Med, 25(7): 595-611.

Duthie SJ, Collins AR. 1997. The influence of cell growth, detoxifying enzymes and DNA repair on hydrogen peroxide-mediated DNA damage (measured using the comet assay) in human cells. Free Radic Biol Med, 22(4): 717-724.

Evans HJ. 1984. Human peripheral blood lymphocytes for the analysis of chromosome aberrations in mutagen tests. In: Kilbey B J, Legator M, Nichols W, Ramel C editors, Handbook of mutagenicity test procedures, Elsevier Sciences, Amsterdam, the Netherlands, pp: 405-424.

Farabaugh CS, Doak S, Roy S, Elespuru R. 2023. In vitro micronucleus assay: Method for assessment of nanomaterials using cytochalasin B. Front Toxicol, 5:1171960.

Fenech M. 2000. The in vitro micronucleus technique. Mutat Res, 455(1): 81-95.

Fenech M. 2007. Cytokinesis-block micronucleus cytome assay. Nat Protoc, 2(5): 1084-1104.

Fenech M. 2020. Cytokinesis-block micronucleus cytome assay evolution into a more comprehensive method to measure chromosomal instability. Genes, 11(10): 1203.

Frawley LE, Orr-Weaver TL. 2015. Polyploidy. Curr Biol, 25(9): R353-R358.

García-Carpintero S, González VJ, Frontiñán-Rubio J, Esteban-Arranz A, Vázquez E, Durán-Prado M. 2023. Screening the micronucleus assay for reliable estimation of the genotoxicity of graphene and other 2D materials. Carbon, 215: 118426.

Gibson DP, Brauninger R, Shaffi HS, Kerckaert GA, LeBoeuf RA, Isfort RJ, Aardema MJ. 1997. Induction of micronuclei in Syrian hamster embryo cells: comparison to results in the SHE cell transformation assay for National Toxicology Program test chemicals. Mutat Res Genet Toxicol Environ Mutagen, 392(1-2): 61-70.

Gopal R, Sharma YK, Shukla AK. 2016. Effect of molybdenum stress on growth, yield and seed quality in black gram. J Plant Nutr, 39(4): 463-469.

Helleday T, Lo J, van Gent DC, Engelward BP. 2007. DNA double-strand break repair: from mechanistic understanding to cancer treatment. DNA Repair, 6(7): 923-935.

Indrakumar J, Korrapati PS. 2020. Steering efficacy of nano molybdenum towards cancer: mechanism of action. Biol Trace Elem Res, 194: 121-134.

Jiang S, Wei J, Li N, Wang Z, Zhang Y, Xu R, Li Y. 2022. The UBP14-CDKB1; 1-CDKG2 cascade controls endoreduplication and cell growth in Arabidopsis. Plant Cell, 34(4): 1308-1325.

Joo SH, Zhao D. 2017. Environmental dynamics of metal oxide nanoparticles in heterogeneous systems: A review. J Hazard Mater, 322: 29-47.

Kailasa SK, Patel MR, Koduru JR, Park TJ. 2024. Recent advances of molybdenum-based nanostructures for molecular and ionic species sensing and separation applications. Coord Chem Rev, 501, 215595.

Kalefetoğlu Macar T, Macar O, Yalçın E, Çavuşoğlu K. 2020. Resveratrol ameliorates the physiological, biochemical, cytogenetic, and anatomical toxicities induced by copper (II) chloride exposure in Allium cepa L. Environ Sci Pollut Res, 27: 657-667.

Kaur J, Kaur K, Pervaiz N, Mehta SK. 2021. Spherical MoO_3 Nanoparticles for Photocatalytic Removal of Eriochrome Black T. ACS Appl Nano Mater, 4(11): 12766-12778.

Khangarot BS. 1991. Toxicity of metals to a freshwater tubificid worm Tubifex tubifex (Muller). Bull Environ Contam Toxicol, 46(6).

Kirsch-Volders M, Plas G, Elhajouji A, Lukamowicz M, Gonzalez L,

Loock KV, Decordier I. 2011. The in vitro MN assay in 2011: origin and fate, biological significance, protocols, high throughput methodologies and toxicological relevance. Arch Toxicol, 85(8): 873-899.

Kizilkaya D, Unal F, Beyzi E, Kulahci MB, Calis Ismetoglu G, Yuzbasioglu D, Suludere Z. 2023. Comparative investigation of iron oxide nanoparticles and microparticles using the in vitro bacterial reverse mutation and in vivo Allium chromosome aberration and comet assays. J Nanopart Res, 25(9): 173.

Kothaplamoottil Sivan S, Padinjareveetil AK, Padil VV, Pilankatta R, George B, Senan C, Varma RS. 2019. Greener assembling of MoO3 nanoparticles supported on gum arabic: cytotoxic effects and catalytic efficacy towards reduction of p-nitrophenol. Clean Technol Environ Policy, 21(8): 1549-1561.

Kumari J, Mangala P. 2022. Fabrication and characterization of molybdenum trioxide nanoparticles and their anticancer, antibacterial and antifungal activities. MJChem, 24(1): 36-53.

Ladon D, Doherty A, Newson R, Turner J, Bhamra M, Case C.P. 2004. Changes in metal levels and chromosome aberrations in the peripheral blood of patients after metal-on-metal hip arthroplasty. J Arthroplasty, 19(8): 78-83.

Li J, Guiney LM, Downing JR, Wang X, Chang CH, Jiang J, Xia T. 2021. Dissolution of 2D molybdenum disulfide generates differential toxicity among liver cell types compared to non-toxic 2D boron nitride effects. Small, 17(25): 2101084.

Libalova H, Zavodna T, Margaryan H, Elzeinova F, Milcova A, Vrbova K, Rössner P. 2024. Differential DNA damage response and cell fate in human lung cells after exposure to genotoxic compounds. In Vitro Toxicol, 94: 105710.

Lorge E, Hayashi M, Albertini S, Kirkland D. 2008. Comparison of different methods for an accurate assessment of cytotoxicity in the in vitro micronucleus test: I. Theoretical aspects. Mutat Res Genet Toxicol Environ Mutagen, 655(1-2): 1–3.

Lunardi CN, Gomes AJ, Rocha FS, De Tommaso J, Patience GS. 2021. Experimental methods in chemical engineering: Zeta potential. The Can J Chem Eng, 99(3): 627-639.

Macar O, Kalefetoğlu Macar T, Çavuşoğlu K, Yalçın E. 2020. Protective effects of anthocyanin-rich bilberry (Vaccinium myrtillus L.) extract against copper (II) chloride toxicity. Environ Sci Pollut Res, 27: 1428-1435.

Magdolenova Z, Collins A, Kumar A, Dhawan A, Stone V, Dusinska M. 2014. Mechanisms of genotoxicity. A review of in vitro and in vivo studies with engineered nanoparticles. Nanotoxicology, 8(3): 233-278.

Mamur S, Yüzbaşıoğlu D, Bülbül SN, Ünal F. 2022. Investigation of cyto-genotoxic effects of a food sweetener Acesulfame potassium. Food and Health, 8(4): 273-283.

Michalová V, Galdíková M, Holečková B, Koleničová S, Schwarzbacherová V. 2020. Micronucleus assay in environmental biomonitoring. Folia Vet, 64(2): 20-28.

Murdock RC, Braydich-Stolle L, Schrand AM, Schlager JJ, Hussain SM. 2008. Characterization of nanomaterial dispersion in solution prior to in vitro exposure using dynamic light scattering technique. Toxicol Sci, 101(2): 239-253.

Nefic H, Handzic I. 2013. The effect of age, sex, and lifestyle factors on micronucleus frequency in peripheral blood lymphocytes of the Bosnian population. Mutat Res Genet Toxicol Environ Mutagen, 753(1): 1-11.

Ngo LP, Kaushal S, Chaim IA, Mazzucato P, Ricciardi C, Samson LD, Engelward BP. 2021. CometChip analysis of human primary lymphocytes enables quantification of inter-individual differences in the kinetics of repair of oxidative DNA damage. Free Radic Biol Med, 174, 89-99.

Nishioka H. (1975). Mutagenic activities of metal compounds in bacteria. Mutat Res, 31(3):185-189.

Nobre FX, Muniz R, Martins F, Silva BO, de Matos JME, da Silva ER, Leyet Y. 2020. Calcium molybdate: Toxicity and genotoxicity assay in Drosophila melanogaster by SMART test. J Mol Struct, 1200: 127096.

NTP. 1997. National Toxicology Program: Molybdenum trioxide. NTP TR 462, NIH Pub. No. 95–3378.

Özkan B, Çavuşoğlu K, Yalçin E, Acar A. 2024. Investigation of multidirectional toxicity induced by high-dose molybdenum exposure with Allium test. Sci Rep, 14(1): 8651.

Palus J, Rydzynski K, Dziubaltowska E, Wyszynska K, Natarajan AT, Nilsson R. 2003. Genotoxic effects of occupational exposure to lead and cadmium. Mutat Res Genet Toxicol Environ Mutagen, 540(1): 19-28.

Raj SG, Rajitha V. 2023. Assessment of genotoxic instability markers in peripheral blood lymphocytes of breast cancer patients: a case control study. Mutat Res Genet Toxicol Environ Mutagen, 42: 1559-1563.

Rodrigues MA, Beaton-Green LA, Wilkins RC, Fenech MF. 2018. The potential for complete automated scoring of the cytokinesis block micronucleus cytome assay using imaging flow cytometry. Mutat Res Genet Toxicol Environ Mutagen, 836: 53-64.

Rossner P, Boffetta P, Ceppi M, Bonassi S, Smerhovsky Z, Landa K, Šrám RJ. 2005. Chromosomal aberrations in lymphocytes of healthy subjects and risk of cancer. Environmental Health Perspectives, 113(5): 517-520.

Saber AT, Mortensen A, Szarek J, Koponen IK, Levin M, Jacobsen NR, Atluri R. 2015. Epoxy composite dusts with and without carbon nanotubes cause similar pulmonary responses, but differences in liver histology in mice following pulmonary deposition. Part Fibre Toxicol, 13(1): 37-57.

Sahoo D, Behera SP, Shakya J, Kaviraj B. 2022. Cost-effective synthesis of 2D molybdenum disulfide (MoS_2) nanocrystals: An exploration of the influence on cellular uptake, cytotoxicity, and bio-imaging. Plos One, 17(1): e0260955.

Santibáñez-Andrade M, Sánchez-Pérez Y, Chirino YI, Morales-Bárcenas R, Quintana-Belmares R, García-Cuellar CM. 2022. Particulate matter (PM10) destabilizes mitotic spindle through downregulation of SETD2 in A549 lung cancer cells. Chemosphere, 295: 133900.

Santos J, Barreto A, Fernandes C, Silva ARR, Cardoso DN, Pinto E, Maria VL. 2023. A comprehensive ecotoxicity study of molybdenum disulfide nanosheets versus bulk form in soil organisms. Nanomaterials, 13(24): 3163.

Santovito A, Cervella P, Delpero M. 2014. Chromosomal damage in peripheral blood lymphocytes from nurses occupationally exposed to chemicals. Hum Exp Toxicol, 33(9): 897-903.

Schins RP, Knaapen AM. 2007. Genotoxicity of poorly soluble particles. Inhal Toxicol, 19: 189-198.

Shao XR, Wei XQ, Song X, Hao L Y, Cai XX, Zhang ZR, Lin YF. 2015. Independent effect of polymeric nanoparticle zeta potential/surface charge, on their cytotoxicity and affinity to cells. Cell Prolif, 48(4): 465-474.

Sharma PK, Raghubanshi AS, Shah K. 2020. Examining dye degradation and antibacterial properties of organically induced α-MoO3 nanoparticles, their uptake and phytotoxicity in rice seedlings. Environ Nanotechnol Monit Manag, 14: 100315.

Sharma PK, Raghubanshi AS, Shah K. 2021. Examining the uptake and bioaccumulation of molybdenum nanoparticles and their effect on antioxidant activities in growing rice seedlings. Environ Sci Pollut Res, 28: 13439-13453.

Siddiqui MA, Saquib Q, Ahamed M, Farshori NN, Ahmad J, Wahab R, Pant AB. 2015. Molybdenum nanoparticles-induced cytotoxicity, oxidative stress, G2/M arrest, and DNA damage in

mouse skin fibroblast cells (L929). Colloids Surf B Biointerfaces, 125: 73-81.

Sikder M, Wang J, Poulin BA, Tfaily MM, Baalousha M. 2020. Nanoparticle size and natural organic matter composition determine aggregation behavior of polyvinylpyrrolidone coated platinum nanoparticles. Environ Sci Nano, 7(11): 3318-3332.

Singh AV, Panchal D, Sharma A, Nandanwar C, Kumar MS, Pal S, Naoghare PK. 2024. Dispersion behaviour of molybdenum disulfide (MoS_2) nanosheets in different exposure media and determination of its toxicity using *in-vitro* ('in vitro' has been italicized) and in-silico approaches. Appl Mater Today, 36: 102023.

Singh NP, McCoy MT, Tice RR, Schneider EL. 1988. A simple technique for quantitation of low levels of DNA damage in individual cells. Exp Cell Res, 175(1): 184-191.

Sobańska Z, Domeradzka-Gajda K, Szparaga M, Grobelny J, Tomaszewska E, Ranoszek-Soliwoda K, Stępnik M. 2020a. Comparative analysis of biological effects of molybdenum (IV) sulfide in the form of nano-and microparticles on human hepatoma HepG2 cells grown in 2D and 3D models. In Vitro Toxicol, 68: 104931.

Sobańska Z, Sitarek K, Gromadzińska J, Świercz R, Szparaga M, Domeradzka-Gajda K, Stępnik M. 2020b. Assessment of acute toxicological effects of molybdenum (IV) disulfide nano-and microparticles after single intratracheal administration in rats. Sci Total Environ, 742: 140545.

Sobańska Z, Sitarek K, Gromadzińska J, Świercz R, Szparaga M, Domeradzka-Gajda K, Stępnik M. 2023. Biological effects of molybdenum (IV) sulfide nanoparticles and microparticles in the rat after repeated intratracheal administration. J Appl Toxicol. 44: 595-608.

Sørli, J.B., Jensen, A.C., Mortensen, A., Szarek, J., Gutierrez, C.A., Givelet, L., Hadrup, N. 2023. Pulmonary toxicity of molybdenum disulphide after inhalation in mice. Toxicology, 447: 153428. https://doi.org/10.1016/j.tox.2023.153428

Struys I, Verscheure E, Lenaerts L, Amant F, Godderis L, Ghosh M. 2023. Characterization of the genotoxic profile of antineoplastic drugs using the cytokinesis-block micronucleus cytome assay. Environ Toxicol Pharmacol, 97: 104036.

Sun K, White JC, He E, Van Gestel CA, Qiu H. 2023. Surface defects regulate the in Vivo bioenergetic response of earthworm Eisenia fetida coelomocytes to molybdenum disulfide nanosheets. ACS Nano, 17(3): 2639-2652.

Terpilowska S, Siwicki AK. 2018. Interactions between chromium (III) and iron (III), molybdenum (III) or nickel (II): Cytotoxicity, genotoxicity and mutagenicity studies. Chemosphere, 201: 780-789.

Titenko-Holland N, Shao J, Zhang L, Xi L, Ngo H, Shang N, Smith MT. 1998. Studies on the genotoxicity of molybdenum salts in human cells in vitro and in mice in vivo. Environ Mol Mutagen, 32(3): 251-259.

Tung GK, Gandhi G. 2023. Baseline and oxidatively damaged DNA in end-stage renal disease patients on varied hemodialysis regimens: a comet assay assessment. Mol Cell Biochem, 479: 199-201.

Uboldi C, Urbán P, Gilliland D, Bajak E, Valsami-Jones E, Ponti J, Rossi F. 2016. Role of the crystalline form of titanium dioxide nanoparticles: Rutile, and not anatase, induces toxic effects in Balb/3T3 mouse fibroblasts. Toxicol in Vitro, 31: 137-145.

Vazquez-Muñoz R, Bogdanchikova N, Huerta-Saquero A. 2020. Beyond the nanomaterials approach: Influence of culture conditions on the stability and antimicrobial activity of silver nanoparticles. ACS Omega, 5(44): 28441-28451.

Verma J, Warsame C, Seenivasagam RK, Katiyar NK, Aleem E, Goel S. 2023. Nanoparticle-mediated cancer cell therapy: Basic science to clinical applications. Cancer Metastasis Rev, 42(3): 601-627.

Vodenkova S, Polivkova Z, Musak L, Smerhovsky Z, Zoubkova H, Sytarova S, Svoboda M. 2015. Structural chromosomal aberrations as potential risk markers in incident cancer patients. Mutagenesis, 30(4): 557-563.

Wang CW, Liang C, Yeh HJ. 2016. Aquatic acute toxicity assessments of molybdenum (+ VI) to Daphnia magna. Chemosphere, 147: 82-87.

Wang J, Sui L, Huang J, Miao L, Nie Y, Wang K, AK. 2021. MoS_2-based ('2' has been superscripted nanocomposites for cancer diagnosis and therapy. Bioact Mater, 6(11): 4209-4242.

Wang S, Li K, Chen Y, Chen H, Ma M, Feng J, Shi J. 2015a. Biocompatible PEGylated MoS_2 nanosheets: controllable bottom-up synthesis and highly efficient photothermal regression of tumor. Biomaterials, 39: 206-217.

Wang X, Mansukhani ND, Guiney LM, Ji Z, Chang CH, Wang M, Nel AE. 2015b. Differences in the toxicological potential of 2D versus aggregated molybdenum disulfide in the lung. Small, 11(38): 5079-5087.

Xing Y, Cai, Cheng J, Xu X. 2020. Applications of molybdenum oxide nanomaterials in the synergistic diagnosis and treatment of tumor. Appl Nanosci, 10(7): 2069-2083.

Yadav U, Singh V, Mishra H, Saxena PS, Srivastava A. 2021. Evaluation of in vitro and in vivo toxicity of pristine molybdenum disulphide nanosheets in Swiss albino mice. BioRxiv, 2021: 05.

Yüzbaşıoğlu D, Çelik M, Yılmaz S, Ünal F, Aksoy H. 2006. Clastogenicity of the fungicide afugan in cultured human lymphocytes. Mutat Res Genet Toxicol Environ Mutagen, 604(1): 53-59.

Zeng J, Hills SA, Ozono E, Diffley JF. 2023. Cyclin E-induced replicative stress drives p53-dependent whole-genome duplication. Cell, 186(3): 528-542. (Paragraph aligned with others)

Zhou Z, Wang Y, Peng F, Meng F, Zha J, Ma L, Tan C. 2022. Intercalation-Activated Layered MoO3 Nanobelts as Biodegradable Nanozymes for Tumor-Specific Photo-Enhanced Catalytic Therapy. Angewandte Chemi, 134(16): e202115939.